Journal of Pharmaceutical Analysis 13 (2023) 239–254

Contents lists available at ScienceDirect

Journal of Pharmaceutical Analysis

journal homepage: www.elsevier.com/locate/jpa

Review paper

Multidisciplinary strategies to enhance therapeutic effects of flavonoids from Epimedii Folium: Integration of herbal medicine, enzyme engineering, and nanotechnology

Yi Lu [a], Qiulan Luo [b, ***], Xiaobin Jia [c], James P. Tam [d], Huan Yang [a], Yuping Shen [a, *], Xin Li [e, f, **]

[a] School of Pharmacy, Jiangsu University, Zhenjiang, Jiangsu, 212013, China
[b] College of Fashion & Design, Jiaxing Nanhu University, Jiaxing, Zhejiang, 314001, China
[c] School of Traditional Chinese Pharmacy, China Pharmaceutical University, Nanjing, 211198, China
[d] School of Biological Sciences, Nanyang Technological University, 637551, Singapore, Singapore
[e] DWI-Leibniz-Institute for Interactive Materials e.V., 52056, Aachen, Germany
[f] Institute for Technical and Macromolecular Chemistry, RWTH Aachen University, 52074, Aachen, Germany

ARTICLE INFO

Article history:
Received 30 August 2022
Received in revised form
29 November 2022
Accepted 27 December 2022
Available online 30 December 2022

Keywords:
Flavonoids
Enzymatic hydrolysis
Nanomedicine
Therapeutic effects
Clinical translation
Epimedii Folium

ABSTRACT

Flavonoids such as baohuoside I and icaritin are the major active compounds in Epimedii Folium (EF) and possess excellent therapeutic effects on various diseases. Encouragingly, in 2022, icaritin soft capsules were approved to reach the market for the treatment of hepatocellular carcinoma (HCC) by National Medical Products Administration (NMPA) of China. Moreover, recent studies demonstrate that icaritin can serve as immune-modulating agent to exert anti-tumor effects. Nonetheless, both production efficiency and clinical applications of epimedium flavonoids have been restrained because of their low content, poor bioavailability, and unfavorable in vivo delivery efficiency. Recently, various strategies, including enzyme engineering and nanotechnology, have been developed to increase productivity and activity, improve delivery efficiency, and enhance therapeutic effects of epimedium flavonoids. In this review, the structure-activity relationship of epimedium flavonoids is described. Then, enzymatic engineering strategies for increasing the productivity of highly active baohuoside I and icaritin are discussed. The nanomedicines for overcoming in vivo delivery barriers and improving therapeutic effects of various diseases are summarized. Finally, the challenges and an outlook on clinical translation of epimedium flavonoids are proposed.

1. Introduction

Epimedium, a genus containing more than 50 species of herbaceous plants, is geographically mainly distributed in China. Fifteen species of *Epimedium* are widely used as traditional Chinese medicine (TCM) and they are well known for "nourishing the kidney and reinforcing the Yang" [1]. Epimedii Folium (EF, Yinyanghuo in Chinese) is the dried leaves of four *Epimedium* plants, including *E. brevicornum* Maxim., *E. sagittatum* (Sieb. et Zucc.) Maxim., *E. pubescens* Maxim., and *E. koreanum* Nakai [2]. Previous phytochemical studies have revealed that diverse components can be extracted from EF, including flavonoids, lignans, xanthones, alkaloids, and acids [3]. Among them, flavonoids are the main active constituents, including epimedin A, epimedin B, epimedin C, icariin, baohuoside I (also known as icariside II), and icaritin [4] (Fig. 1). These flavonoids, especially icariin, baohuoside I, and icaritin, show enormous potential in treatment of various diseases, such as osteoarthritis, cardiovascular disease, diabetes, male sexual dysfunction, neurodegenerative disorders, inflammation, Alzheimer's disease, and cancers [1]. Icariin, the most abundant active component in EF, has been recognized as a quality-control marker for EF [5,6]. Recent icariin metabolism studies have reported that icariin is transformed to baohuoside I and icaritin in vivo, which can be absorbed in small intestine [7]. Moreover, compared with icariin, baohuoside I and icaritin display stronger

Peer review under responsibility of Xi'an Jiaotong University.
* Corresponding author.
** Corresponding author. DWI-Leibniz-Institute for Interactive Materials e.V., 52056 Aachen, Germany.
*** Corresponding author.
E-mail addresses: 202202@jxnhu.edu.cn (Q. Luo), syp131@ujs.edu.cn (Y. Shen), xli@dwi.rwth-aachen.de (X. Li).

https://doi.org/10.1016/j.jpha.2022.12.001

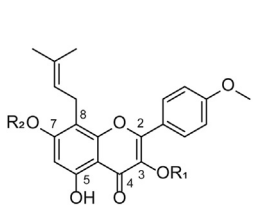

R_1	R_2	Compounds
Rha	Glc	Icaritin
Rha²-Glc	Glc	Epimedin A
Rha²-Xyl	Glc	Epimedin B
Rha²-Rha	Glc	Epimedin C
Rha	H	Baohuoside I
Rha²-Glc	H	Sagittatoside A
Rha²-Xyl	H	Sagittatoside B
Rha²-Rha	H	2″-*o*-rhamnosyl icariside II
H	H	Icaritin

Fig. 1. Chemical structures of flavonoids from Epimedii Folium (EF). glc: glucose; rha: rhamnose; xyl: xylose.

biological activities, such as the differentiation and proliferation of osteoblasts [8,9].

Notably, in 2022, icaritin soft capsules, as a novel immunomodulatory antitumor agent, were approved to reach the market for the treatment of hepatocellular carcinoma (HCC) by National Medical Products Administration (NMPA) of China based on the favorable results of phase III clinical trials (NCT03236636, NCT03236649) [10]. However, the contents of baohuoside I (<0.3%) and icaritin (<0.1%) in EF were too low to achieve large-scale production by the conventional extraction technology [11,12]. Therefore, it is important to develop effective methods to convert the abundant icariin or the total flavonoid extract of *epimedium* (TFEE) into more active baohuoside I and icaritin. Moreover, it is also crucial to further investigate the pharmaceutical properties and promote the biomedical applications of baohuoside I and icaritin. Despite tremendous progress and efforts in determining the activities of baohuoside I and icaritin, their clinical applications remain restricted due to their low bioavailability and inefficient delivery in vivo [13,14]. Thus, it is essential to develop powerful strategies that can address the existing issues related to baohuoside I and icaritin, as well as fully exerting their therapeutic effects.

In recent years, extensive efforts have been devoted to preparing baohuoside I and icaritin, such as column chromatography, chemical synthesis, chemical hydrolysis, and enzymatic hydrolysis. The application of column chromatography in the large-scale production of these two flavonoids is limited due to their low content in EF [15]. Chemical synthesis of icaritin demands harsh reaction conditions, such as high temperature, which have hindered its scale-up and commercial applications [16]. In addition, the chemical hydrolysis method often has some negative effects on the activities of products and generates byproducts. Alternatively, enzymatic hydrolysis methods are widely utilized due to their significant advantages of remarkable selectivity, mild conditions, high efficiency, and environmental protection. For instance, Liu et al. [12] applied efficient and clean enzymatic hydrolysis method to produce icaritin from epimedin C with immobilized α-L-rhamnosidase and β-glucosidase. In the process of enzymatic hydrolysis, the catalytic efficiency and yield of hydrolysates can be improved by optimizing enzyme properties, substrate solubility, and hydrolysis conditions and systems [17].

Nanoparticles (NPs) can be applied to enhance the bioavailability and delivery efficiency of baohuoside I and icaritin. NPs have unique properties such as high surface area and beneficial physicochemical characteristics, which can enable them to modulate the pharmacokinetic and pharmacodynamic profiles of the loaded bioactive compounds [18]. Loading flavonoids into NPs can increase their stability, solubility and permeability, prolong drug blood circulation, augment targeted delivery, elevate tumor penetration, and overcome multidrug resistance (MDR) [19]. Owing to these benefits, therapeutic effects such as anti-osteonecrosis and antitumor effects of these nanomedicines have been confirmed to be superior to those of free drugs [20,21].

This review summarizes the recent advances in the preparation of baohuoside I/icaritin, and the delivery as well as the applications of their nanomedicines (Fig. 2). We first introduce the structures, therapeutic goals, and structure-activity relationship (SAR) of three flavonoids, namely, icariin, baohuoside I, and icaritin. Second, we summarize several optimized enzymatic hydrolysis methods to obtain highly active baohuoside I and icaritin from the aspects of improving enzyme properties, substrate solubility, and hydrolysis conditions and systems. Furthermore, we present a number of smart NPs to enhance the bioavailability, prolong blood circulation, augment target delivery, elevate tumor penetration, and overcome MDR of baohuoside I/icaritin; the applications of these nanomedicines in the treatment of cancers and osteonecrosis are also described. Finally, we conclude this review with solutions to challenges existing in the production of baohuoside I/icaritin and applications of their nanomedicines, and future prospects for their clinical practice are also provided. To our knowledge, this is the first comprehensive review to summarize the latest achievements and propose new opportunities as well as future challenges in the field of epimedium flavonoids for improving the therapeutic effects of baohuoside I/icaritin on various diseases.

2. SAR of flavonoids from EF

Flavonoids are the main active ingredients of EF and have excellent pharmacological activities against osteoporosis, cardiovascular diseases, sexual dysfunction, inflammation, and cancers [1]. Based on cumulative findings concerning the SAR of flavonoids, it is reasonable to infer that the prenyl side chain position at C-8, double bond of the C2=C3, 4-carbonyl group, and hydroxylation patterns, especially 3-OH, play a significant role in the therapeutic effects of flavonoids [22]. The prenyl side chain position at C-8 is key to the cytotoxic activities on human cancer cells, anti-inflammatory activity, and inhibitory activity toward some enzymes like 3′,5′-cyclic monophosphate and phosphodiesterase 5 (cGMP-PDE5) [23]. cGMP-PDE5 plays an important role in modulating smooth muscle tone in general, and the inhibitors of cGMP-PDE5 can be used to treat erectile dysfunction. Additionally, the double bond of C2=C3 and the 4-carbonyl group are beneficial to diverse activities, such as antiviral/bacterial, anticancer, anti-neuropathology, cardioprotective, anti-inflammatory, anti-diabetes, and antioxidant activities [22]. Similarly, 3-OH contributes to a variety of activities except for antidiabetes. Generally, the glycosylation of flavonoids may increase the corresponding antiviral/bacterial activity, but is anti-age-dependent on the contrary.

Specifically, icariin, baohuoside I, and icaritin, the main active flavonoids in TFEE, exert therapeutic effects on various diseases (Table 1 [24–57] and Table S1 [58–73]). Icariin is the most abundant flavonoid in EF, while the natural contents of baohuoside I and icaritin are very low [74]. The contents of these three flavonoids in EF are affected by species, growth conditions, and flavonoid extraction methods [75,76]. For example, the contents of icariin and baohuoside I vary in different species of EF (Fig. S1) [15]. As the most abundant active component in EF, icariin, is shown to possess multiple pharmacological effects against osteoarthritis and cartilage injury, myocardial ischemia, and inflammation [58,77]. Icariin can also serve as an alternative drug for the therapy of cancers and other diseases, such as male sexual dysfunction, Alzheimer's disease, and acute promyelocytic leukemia [68,78]. Remarkably, baohuoside I and icaritin display higher bioactivity and therapeutic effects than icariin [38,46]. For example, baohuoside I and icaritin have better bioavailability and more excellent effects for osteogenic differentiation and proliferation [79].

It was reported that the higher pharmaceutical activities of baohuoside I and icaritin arose from reduced sugar moieties in

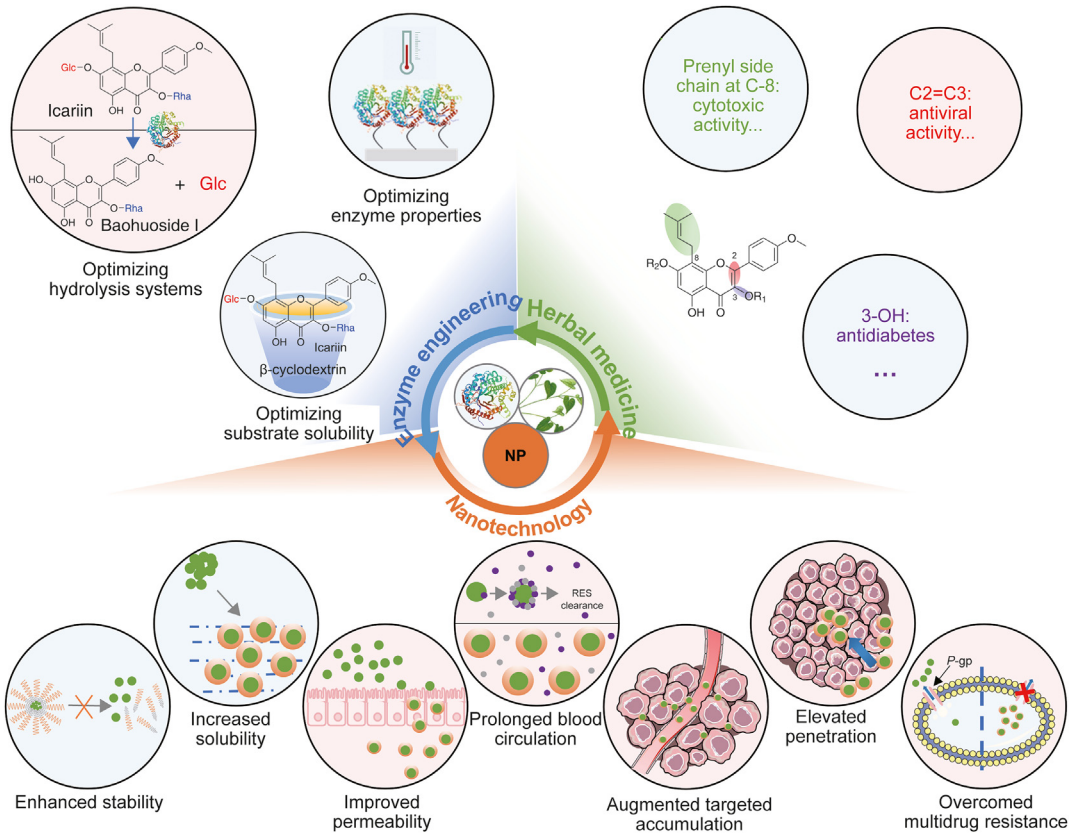

Fig. 2. Integration of herbal medicine, enzyme engineering, and nanotechnology for increasing productivity and activity, improving delivery efficiency in vivo, and enhancing therapeutic effects of epimedium flavonoids. NP: nanoparticle; Glc: glucose; Rha: rhamnose; RES: reticuloendothelial system; *P*-gp: *P*-glycoprotein.

contrast to icariin [80]. With respect to structures (Fig. 1), these three flavonoids have the same fundamental skeleton but different glycosyl substitutions at the C-3 and C-7 positions [80]. Icariin possesses a glucose group at the 7-O position and an additional rhamnose moiety at the 3-O position [81]. Unlike icariin, baohuoside I only has a rhamnose moiety at the 3-O position, and icaritin is the aglycone of epimedium flavonoids without any sugar moieties. Except for extraction from EF, baohuoside I can also be obtained by releasing the sugar moieties at the C-7 position of icariin [80]. Icaritin can be produced by deglycosylation at both the C-3 and C-7 positions from TFEE, including icariin and epimedin A/B/C [8,80].

3. Preparation of baohuoside I and icaritin by enzymatic hydrolysis

In recent decades, column chromatography, chemical synthesis, chemical hydrolysis, and enzymatic hydrolysis have been employed to obtain baohuoside I and icaritin. Among these approaches, enzymatic hydrolysis has demonstrated enormous potential in the preparation of baohuoside I and icaritin owing to its remarkable selectivity, mild reaction conditions, high efficiency, and environmental friendliness [17].

To produce baohuoside I, β-glucosidase, dextranase, and cellulose are employed to remove glucose from the 7-O position of icariin [82]. In addition, the aglycone icaritin can be generated by releasing all the sugar moieties from several flavonoids (e.g., icariin and baohuoside I) using snailase or a mixture of β-glucosidase and α-L-rhamnosidase [12,83]. However, the enzymatic transformation efficiency was still restricted by the low activity and poor stability of enzymes, difficulties in recycling enzymes, unsatisfactory solubility of substrates, and inadequate catalytic conditions. To improve the hydrolysis efficiency, the enzyme properties, substrate solubility, hydrolysis conditions and systems were optimized (Table S2) [84–99].

3.1. Utilization of ameliorated enzymes

Enzyme properties are pivotal in the enzymatic hydrolysis of flavonoids. To address the problems of low stability, methods of improving enzyme thermostability and enzyme immobilization technology are exploited to increase the hydrolytic efficiency and reusability. In addition, the catalytic efficiency of substrates with poor water solubility can be improved through the utilization of organic solvent-tolerant enzymes [99]. Since feedback inhibition of sugars impairs the hydrolysis efficiency of glycosidases, enzymes with high sugar resistance can also increase the productivity of flavonoids [99].

In previous work, β-glucosidase, dextranase, and cellulase have been applied to produce baohuoside I by removing glucose from the 7-O position of icariin [85–90,92]. Recently, a novel GH1 β-glucosidase with high thermostability, IagBgl1, was produced for the transformation of icariin into baohuoside I [85]. It displayed high conversion efficiency during the production of baohuoside I because its remarkable thermostability improved the substrate solubility and mass transfer and reduced the risk of contamination. The recombinant IagBgl1 performed well at a high reaction temperature and showed outstanding thermostability. The optimized hydrolysis temperature was observed at 95 °C, and the residual

Table 1
The therapeutic effects of baohuoside I and icaritin.

Compounds	Structure		Therapeutic effects	Research model	Dosage	Refs.
	R_1	R_2				
Baohuoside I (Icariside II)	Rha	H	Osteoporosis	Rat model of osteoporosis	5, 25, and 50 μM/L/kg	[24]
			Osteosarcoma	Osteosarcoma cell model	0.1, 1, and 10 μM	[25]
			Cerebral ischemia/reperfusion	Rat model of middle cerebral artery occlusion	16 mg/kg	[26]
			Myocardial ischemia and reperfusion injury	Rat model of myocardial ischemia and reperfusion injury	10, 20, and 30 mg/kg	[27]
			Diabetes	Rat model of streptozotocin-induced diabetes	5 mg/kg	[28]
			Erectile dysfunction	Rat model of erectile dysfunction	2.5 mg/kg	[29]
			Alzheimer's disease	Mice model of Alzheimer's disease	10, and 30 mg/kg	[30]
			Neuroinflammation	Rat model of lipopolysaccharide-induced neuroinflammation	10 mg/kg	[31]
			Airway inflammation	Mice model of eosinophils-induced airway inflammation	10, and 30 mg/kg	[32]
			Multiple myeloma	Mice model of multiple myeloma	25 mg/kg	[33]
			Prostate cancer	Prostate cancer cell model	10, 20, and 40 μM	[34]
			Non-small cell lung cancer	Mice model of non-small cell lung cancer	10 mg/kg	[35]
			Cervical cancer	Mice model of cervical cancer	25 mg/kg	[36]
			Breast cancer	Mice model of breast cancer	10, and 20 mg/kg	[37]
			Pancreatic cancer	Pancreatic cancer cell model	10–90 μM	[38]
			Hepatocellular carcinoma	Mouse model of hepatocellular carcinoma	25 mg/kg	[39]
			Nasopharyngeal carcinoma	Mice model of nasopharyngeal carcinoma	25 mg/kg	[40]
			Glioma	Mice model of glioma	35 mg/kg	[41]
			Melanoma	Mice model of melanoma	25 mg/kg	[42]
Icaritin	H	H	Osteonecrosis	Rat model of steroid-associated osteonecrosis	16 mg/kg	[43]
			Myocardial ischemia	Rat model of myocardial ischemia-reperfusion	3, 10, and 30 mg/kg	[44]
			Multiple myeloma	Mice model of multiple myeloma	3, and 6 mg/kg	[45]
			Liver fibrosis	Rat model of hepatic fibrosis	1 mg/kg	[46]
			Neuroinflammation	Mice model of neuroinflammation	20 mg/kg	[47]
			Parkinson's disease	Mouse model of Parkinson's disease	4.7, 9.5, and 18.9 mg/kg	[48]
			Cervical cancer	Cervical cancer cell model	3–80 μM	[49]
			Breast cancer	Mouse model of breast cancer	50 mg/kg	[50]
			Prostate cancer	Mice model of prostate cancer	33 mg/kg	[51]
			Ovarian cancer	Mice model of ovarian cancer	33 mg/kg	[52]
			Bladder cancer	Bladder cancer cell model	2.5–50 μM	[53]
			Colorectal cancer	Mice model of colorectal cancer	25 mg/kg	[54]
			Gliomas	Glioblastoma multiforme cell model	5, 10, and 20 μM	[55]
			Hematological malignancies	Mouse model of hematological malignancies	4, and 8 mg/kg	[56]
			Hepatocellular carcinoma	Mouse model of hepatocellular carcinoma	5 mg/kg	[57]

Rha: rhamnose.

activity was higher than 70% after incubation at 90 °C for 4 h. In addition, this enzyme also exhibited high tolerance to sugar and organic solvents, as supported by more than 90% residual activity with concentrations of methanol below 15% and an excellent glucose tolerance (*Ki*) of approximately 1600 mM. Moreover, IagBgl1 exhibited a high catalytic activity toward icariin with a K_{cat}/K_m ratio of 488.19 $mM^{-1}\cdot s^{-1}$. Finally, icariin was hydrolyzed into baohuoside I with a high molar conversion of 99.48% under optimized conditions.

The production of icaritin can be achieved by the hydrolysis of the glycosidic bond at the C-3 and C-7 positions of major flavonoids, such as icariin and epimedin A/B/C [88,100]. Similar to the preparation of baohuoside I, the sugar moiety at the C-7 position can be degraded by β-glucosidase [88]. Meanwhile, the glycosidic bond at the C-3 position needs to be hydrolyzed by α-L-rhamnosidases. However, few of α-L-rhamnosidases have been employed in the removal of rhamnose residue at the C-3 position [88]. Recently, a novel α-L-rhamnosidase (Rhase-I) from *Talaromyces stollii* CLY-6 was used to produce icaritin from epimedin C together with the β-glucosidase Bglsk [96]. Rhase-I was verified to hydrolyze the α-1,2-glycosidic linkage between aglycone and rhamnose as well as the two rhamnose moieties in epimedin C, which was the prerequisite for preparing icaritin from epimedin C (Figs. 3A and B) [96]. In addition, the binding mechanism between Rhase-I and epimedin C was predicted via computational analysis, revealing the hydrogen-bond and hydrophobic interactions between several amino acids of Rhase-I and epimedin C (Fig. 3C). Rhase-I required a moderate reaction temperature and showed high thermal and pH stability, indicating its promising potential in the scaled-up production of icaritin (Figs. 3D and E). To efficiently produce icaritin, a two-step enzymatic hydrolysis method was established, and the highest icaritin productivity of Rhase-I ever reported of up to 93.16 g/L/h/g was achieved (Fig. 3F).

In addition, enzyme immobilization technology is also an alternative to improve hydrolysis efficiency. In comparison to free enzymes, immobilized enzymes are more stable and resistant to environmental changes. Moreover, the immobilized enzymes can be easily separated from the reaction solution and reused for several times, which simplifies the operation procedures and reduces the production cost. For instance, snailase was immobilized on glutaraldehyde-activated aminated silica (SiO_2—NH_2-GA) NPs by covalent binding for the transformation of the epimedium flavonoids [97]. In contrast to free snailase, the immobilized snailase displayed good hydrolysis capacity, improved pH and thermal tolerance, and excellent stability. The immobilized snailase retained more than 60% of the original activity after six times of repeated use. Moreover, the hydrolysates produced by the immobilized snailase, including baohuoside I, showed excellent antitumor efficacy. Dong et al. [98] reported the immobilization of two thermostable glycosidases, β-glucosidase DthBgl3 and α-L-rhamnosidase DthRha, on 1000NH amino resin and investigated their cooperative hydrolysis efficiency of all major ingredients of TFEE. The results demonstrated that all major ingredients in 10 g/L TFEE were completely transformed into icaritin in 2 h at pH 6.0 and 85 °C by the two immobilized enzymes. A molar conversion rate of 87.21% and icaritin's productivity of 141 mg/L/h were reached by the hydrolysis of two immobilized enzymes after 15 times of repeated use.

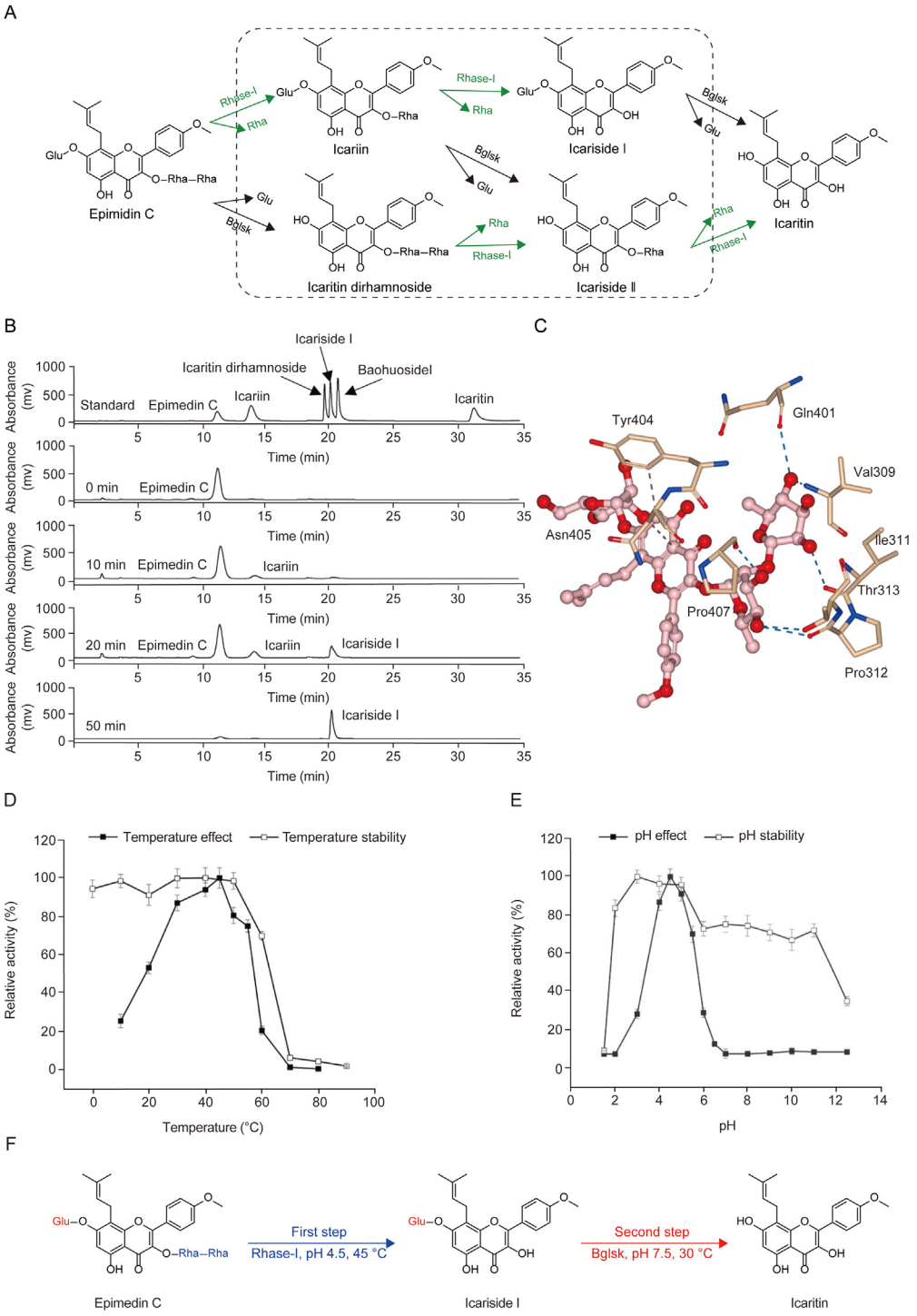

Fig. 3. Utilization of Rhase-I and Bglsk for preparing icaritin from epimedin C. (A) Conversion pathway of epimedin C to icaritin by Rhase-I and Bglsk. (B) Hydrolysates from epimedin C by Rhase-I with different reaction times analyzed by high-performance liquid chromatography (HPLC). (C) Binding of epimedin C and several amino acids of Rhase-I including Val 309, Ile 311, Pro 312, Thr313, Gln 401, and Pro 407 via hydrogen-bond interactions, and Tyr404 and Asn 405 via hydrophobic interactions. (D, E) Effects of temperature (D) and pH (E) on Rhase-I. (F) Enzymatic hydrolysis of epimedin C to icaritin in two steps. Reprinted from Ref. [96] with permission. Rha: rhamnose; Glu: glucose; Val: valine; Ile: isoleucine; Pro: proline; Thr: threonine; Gln: glutamine; Tyr: tyrosine; Asn: asparagine.

3.2. Improvement of substrate solubility

Although enzymatic hydrolysis efficiency can be improved by applying enzymes with superior properties, the contact of enzymes with flavonoids is still insufficient because of the low aqueous solubility of flavonoids. Therefore, it is valuable to develop an approach to improve the aqueous solubility of substates and consequently increase the chances of interaction between these substrates and enzymes.

β-cyclodextrin, a cyclic oligosaccharide, consists of hydrophilic outer tails and hydrophobic inner cavities [95]. Because of its relatively lipophilic surface of the internal cavity, β-cyclodextrin

can easily form inclusion complexes with poorly aqueous-soluble drugs to enhance their solubility [101,102]. For the purpose of highly efficient production of icaritin, our group prepared an icariin/β-cyclodextrin inclusion complex and performed enzymic hydrolysis by snailase [95]. As a result, the solubility of icariin was increased by 17 times from 29.2 μg/mL to 513.5 μg/mL at 60 °C. Moreover, the reaction time was decreased by 68% during icaritin preparation compared with that without the β-cyclodextrin complex. Additionally, it was reported that the solubility of the icariin nanosuspension was 50 times higher than that of free icariin, indicating that enzymatic hydrolysis efficiency can be enhanced by utilizing a substrate nanosuspension [103].

3.3. Optimization of hydrolysis conditions and enzymatic systems

Apart from the aforementioned enzyme properties and substrate solubility, the hydrolysis efficiency can be improved by optimizing hydrolysis conditions or systems. During the enzymatic catalysis of icariin, many factors, such as the reaction time, temperature, pH value, and the ratio of substrate/enzyme, impact the conversion efficiency. To improve enzymatic hydrolysis efficiency, reaction parameters were optimized by orthogonal array design, central composite design (CCD), and uniform design coupled with subset selection [86,90,91]. For instance, three parameters, i.e., the initial substrate concentration, pH and temperature, were optimized to achieve a high conversion rate of icariin by the CCD model, and applied in the enlarged baohuoside I production [86]. With the optimized conditions of pH at 4.0, temperature of 41 °C, 1.0 mg/mL icariin, and 9.8 U/mL crude β-glucosidase, the conversion rate reached up to 95.03% in 1 h. In addition, the produced baohuoside I exhibited superior inhibitory effects on the proliferation of A549 cells than icariin.

Additionally, a biphase enzymatic hydrolysis system for the transformation of icariin into baohuoside I was established with the advantages of improved production convenience and enzyme reusability. In our previous work, two phases were formed by covering the aqueous phase, where enzymatic hydrolysis of icaritin occurred, with hydrophobic organic solvent (Fig. 4) [92]. In the system, icariin was distributed to both phases before hydrolysis due to its poor water solubility. During enzymatic catalysis, icariin dissolved in the aqueous phase was converted to baohuoside I by β-glucosidase, and then the formed baohuoside I with lower polarity was extracted to the organic phase. Extraction of the product ensured the reversible hydrolysis reaction to proceed, which promoted more icariin to move from the organic phase into the aqueous solution. Compared with the conventional enzymatic hydrolysis (single phase), the newly designed biphase enzymatic hydrolysis system improved the process capacity of icariin and realized the reuse of enzymes. The processing capacity of this novel biphase hydrolysis system was 2.5 times that of the conventional enzymatic hydrolysis method, and an up to 85% conversion rate was obtained after three times use of the enzyme solution.

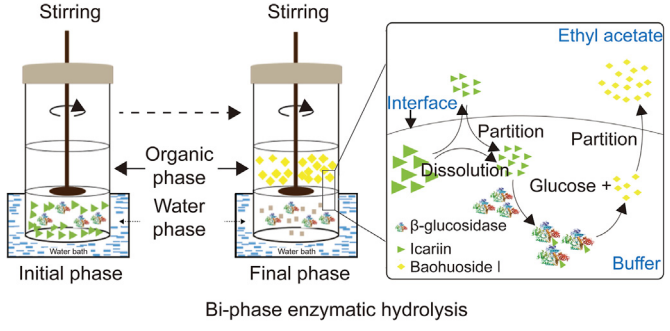

Fig. 4. Diagram of the biphase enzymatic hydrolysis process. In the biphase enzymatic hydrolysis system, icariin dissolved in the aqueous phase was hydrolyzed by β-glucosidase and the product baohuoside I was extracted to the organic phase. The transfer of the product into the organic phase accelerated the catalysis of icariin and the dissolution of icariin from the organic phase into buffer. Reprinted from Ref. [92] with permission.

Overall, the enzymatic hydrolysis method is a promising approach to prepare baohuoside I or icaritin on a large scale. Since the activity of enzymes would be decreased during long-term reaction, combining several strategies aforementioned, such as conducting enzymatic catalysis of icariin by immobilized β-glucosidase and α-L-rhamnosidase variants in a biphase enzymatic hydrolysis system would further improve the enzymatic hydrolysis efficiency and thus increase the productivity of baohuoside I or icaritin.

4. Engineering of flavonoids by nanotechnology

Although various enzymatic hydrolysis strategies have been developed to efficiently convert icariin or TFEE to baohuoside I and icaritin, their clinical applications are still limited due to their low bioavailability, short blood circulation, unsatisfory targeting and penetration, and inevitable MDR. Recently, nanotechnology has presented great potential to address these challenges of baohuoside I and icaritin and shows unrivalled advantages [104–106]. First, loading baohuoside I and icaritin into NPs can improve their stability, reduce their toxicity via the protection of NPs, and avoid exposure in the physiological environment. Due to the unique properties of NPs, they can improve the solubility and permeability of the encapsulated drugs and thereby enhance their bioavailability [107]. Additionally, the NPs can also target their cargoes to specific tissues or cells either passively or actively [108]. Moreover, NPs can prolong the blood circulation, augment target delivery, elevate tumor penetration, and overcome the MDR of baohuoside I and icaritin by optimizing the size, shape, charge, and functionalized decoration of NPs.

The encapsulation efficiency of baohuoside I or icaritin-loaded NPs depends on the polarity, size, and partition coefficient of baohuoside I or icaritin as well as the properties of the NPs. Baohuoside I and icaritin are hydrophobic and are loaded into NPs mainly through hydrophobic interactions. For instance, baohuoside I or icaritin was encapsulated in the acyl hydrocarbon chain of the liposome, and the encapsulation efficiency relied on the properties of baohuoside I or icaritin and the acyl chains of the liposome, such as the length and packing density [109,110]. Likewise, many methods have been developed to prepare baohuoside I- or icaritin-loaded NPs, including the acid-base shift method, thin film hydration, extrusion, and sonication [14,111–114].

4.1. Enhanced stability

NPs can enhance the stability of drugs by preventing them from degradation in adverse external environments such as low pH and enzymes. For instance, NPs can improve the capacity of oral drugs to withstand the low pH and digestive enzyme environment in the gastrointestinal tract (GIT) before reaching the drug absorption site. However, some kinds of NPs, such as micelles and liposomes, show low stability because of their inherent structural properties. Many efforts have been devoted to improving their stability, such as the utilization of more stable polymeric micelles and modification of liposome composition [110,115].

Polymeric micelles are formed by block copolymers and consist of two distinct sections, a hydrophobic core and a hydrophilic shell. They are quite stable in physiological media while the hydrophilic shell protects the encapsulated drug from the external environment [116]. For example, the mixed Soluplus® and Poloxamer 407 (P407)

were selected to produce polymeric micelles due to their favorable low critical micelle concentration (CMC) value of 7.9 mg/L by a creative acid-base shift method (Fig. 5A) [115]. With this method, icaritin was first dissolved in NaOH aqueous solution in a salt form due to its weak acidity with phenolic hydroxyl groups (Ar-OH). Then, the solution of Soluplus®/P407 in HCl was added to the icaritin solution. During the process of addition, the soluble salt of icaritin was transformed to free icaritin and was simultaneously encapsulated in the hydrophobic core of the micelles. The formed icaritin-loaded polymeric micelles (IPMs) were endowed with excellent dilution-resistant stability in the GIT due to the low CMC value of Soluplus® and P407. At first, IPMs displayed high chemical stability, as the purity of the loaded icaritin was measured as 99.5% by high-performance liquid chromatography (HPLC). The prepared IPMs exhibited a small size in the range of 63–99 nm with a narrow distribution (polydispersity index (PDI) < 0.2) (Figs. 5B and C). In addition, the IPMs could be stored at 4 °C for up to 8 weeks without any obvious change in the size, PDI, or icaritin loading content (Fig. 5D). There was also no remarkable fluctuation in these parameters of concentrated IPMs upon a 25-fold dilution with simulated gastric fluid (SGF) and simulated intestinal fluid (SIF) at 37 °C (Fig. 5E). Furthermore, the pharmacokinetic studies showed that the bioavailability for IPMs was 14.9-fold higher than that of the clinical icaritin formulation (oil suspension) (Table S3) [115].

In terms of improving the stability of micelles, many researchers have explored the possibility of improving the stability of liposomes by modifying the components of bilayers [117]. It has been reported that the stability of liposomes can be easily modified by the adequate addition of surfactants [118]. For instance, Tai et al. [110] investigated the effects of four kinds of surfactants, namely, Span 40, Span 20, sucrose ester and Tween 80, on the physical and thermal stability of icaritin-loaded liposomes. The icaritin-loaded liposomes were produced by the thin film hydration method and subsequent ultrasonic processing. As a result, the turbiscan stability index (TSI) value of cholesterol-free icaritin-loaded liposomes with Span 40 (<0.1 within storage for 200 min) was significantly lower than that of liposomes with other surfactants. In addition, liposomes supplemented Tween 80 displayed higher heat stability and stronger protective effects for icaritin since hardly any icaritin leaked after 8 h when they were heated at 55 °C. All the aforementioned evidence indicated that surfactants could further enhance the physical and thermal stability of liposomes.

4.2. Increased solubility and dissolution rate

The poor solubility and low dissolution rate are the main factors contributing to the low bioavailability of baohuoside I and icaritin. The water solubilities of icaritin and baohuoside I are below 1 and 15 μg/mL, resulting in their dissatisfactory bioavailability of approximately 2% [119,120].

The formulation of drug nanocrystals and encapsulation of drugs into hydrophobic parts of mixed micelles, liposomes, and polymeric NPs can efficiently increase their solubility [8,120]. For instance, icaritin nanocrystals showed a higher dissolution rate and improved bioavailability compared with unformulated icaritin owing to the high surface area of nanocrystals [8]. Additionally, mixed micelles can be applied to significantly improve the drug solubility due to the manifested synergistic properties of the micelle components. In our previous work, a phospholipid complex and D-α-tocopheryl polyethylene glycol 1000 succinate (TPGS) mixed micelles were used to improve the oral absorption of baohuoside I [13]. The preparation of mixed micelles was divided into two steps. The baohuoside I-phospholipid complex was first produced using an anhydrous cosolvent reduction vaporization method. Then, mixed micelles composed of the baohuoside I-phospholipid complex and TPGS were obtained by the solvent evaporation method. As a result, the solubility of baohuoside I was increased by the mixed micelles. In particular, at a TPGS/baohuoside I–phospholipid complex molar ratio of 9:1, the solubility of baohuoside I reached 1124.5 μg/mL, which was almost 87 times higher than that of free baohuoside I (12.8 μg/mL), leading to the increase in area under curve ($AUC_{0-\infty}$) (mg/L·min) of baohuoside I from 74.12 ± 10.02 (free baohuoside I) to 395.15 ± 62.39 (baohuoside I-loaded micelles). The improved solubility was caused by the role of TPGS and the strong interaction between TPGS and the baohuoside I-phospholipid complex.

4.3. Improved permeability

Apart from solubility, drug permeability is also significant for bioavailability. Only by maintaining an optimal solubility-permeability tradeoff can the bioavailability of drugs be substantially improved. For oral drugs, the small intestine is the main absorption site, and loading drugs with NPs is deemed to be an ideal strategy to improve their permeability [121]. For example, our group produced baohuoside I-phospholipid complexes by a reduction vaporization method and determined their permeability [122]. In contrast to free baohuoside I, improved permeability of baohuoside I-phospholipid complexes (280% of free baohuoside I for baohuoside I-phospholipid complexes with a size of 81 ± 10 nm) was observed since the interaction between complexes and the cell membrane was strengthened by phospholipids.

4.4. Prolonged blood circulation

During blood circulation, easy drug degradation caused by enzymes, pH, and other factors leads to a short half-life of drugs. NPs have been used to load various types of drugs and prevent them from degradation. Several strategies have been designed to further prolong the blood circulation of drug-loaded NPs by adjusting the size, shape, charge, and surface modification of the NPs [123].

To avoid renal excretion and reticuloendothelial system (RES) clearance, spherical particles with diameters between 100–200 nm are appropriate for long-circulating NPs [124]. With regard to surface charge, neutral and slightly negative NPs have a prolonged circulation time [125]. In addition, surface decoration of NPs with some hydrophilic polymers, such as polyethylene glycol (PEG) and polysaccharides, can prevent the rapid removal of NPs since RES clearance can be relieved by reducing hydrophobic interactions between opsonizing proteins and NPs [123]. Likewise, zwitterionic NPs have highly hydrophilic surfaces due to their superior ionic solvation with water molecules [126–128]. Thus, zwitterionic NPs can also increase the blood circulation time by reducing protein absorption.

To achieve higher performance, a proper combination of several strategies above is needed. For instance, Yu et al. [57] prepared the icaritin and doxorubicin (DOX)-loaded poly(lactic-*co*-glycolic acid) (PLGA) NPs for HCC immunotherapy. As shown in Fig. 6A, the PLGA-PEG-AEEA-DOX/icaritin NPs were developed using the solvent displacement technique. The drugs (icaritin and DOX) and NPs (PLGA-PEG and PLGA-PEG-AEAA) were first dissolved in dimethyl sulfoxide (DMSO). Then, they were mixed, and the DMSO was replaced with H_2O, leading to the formation of PLGA-PEG-AEEA-DOX/icaritin NPs. The prepared DOX/icaritin-loaded NPs had a size of appropriately 100 nm (Figs. 6B and C). Because of the befitting size and PEGylation, compared with the free drugs, both icaritin and DOX formulated NPs showed a lower clear rate in the blood (Fig. 6D). The half-life time ($t_{1/2}$) of icaritin and DOX was apparently increased from 0.41 or 0.14 h for the free types to 1.65 or 1.96 h for the coformulation types, respectively (Table S4) [57].

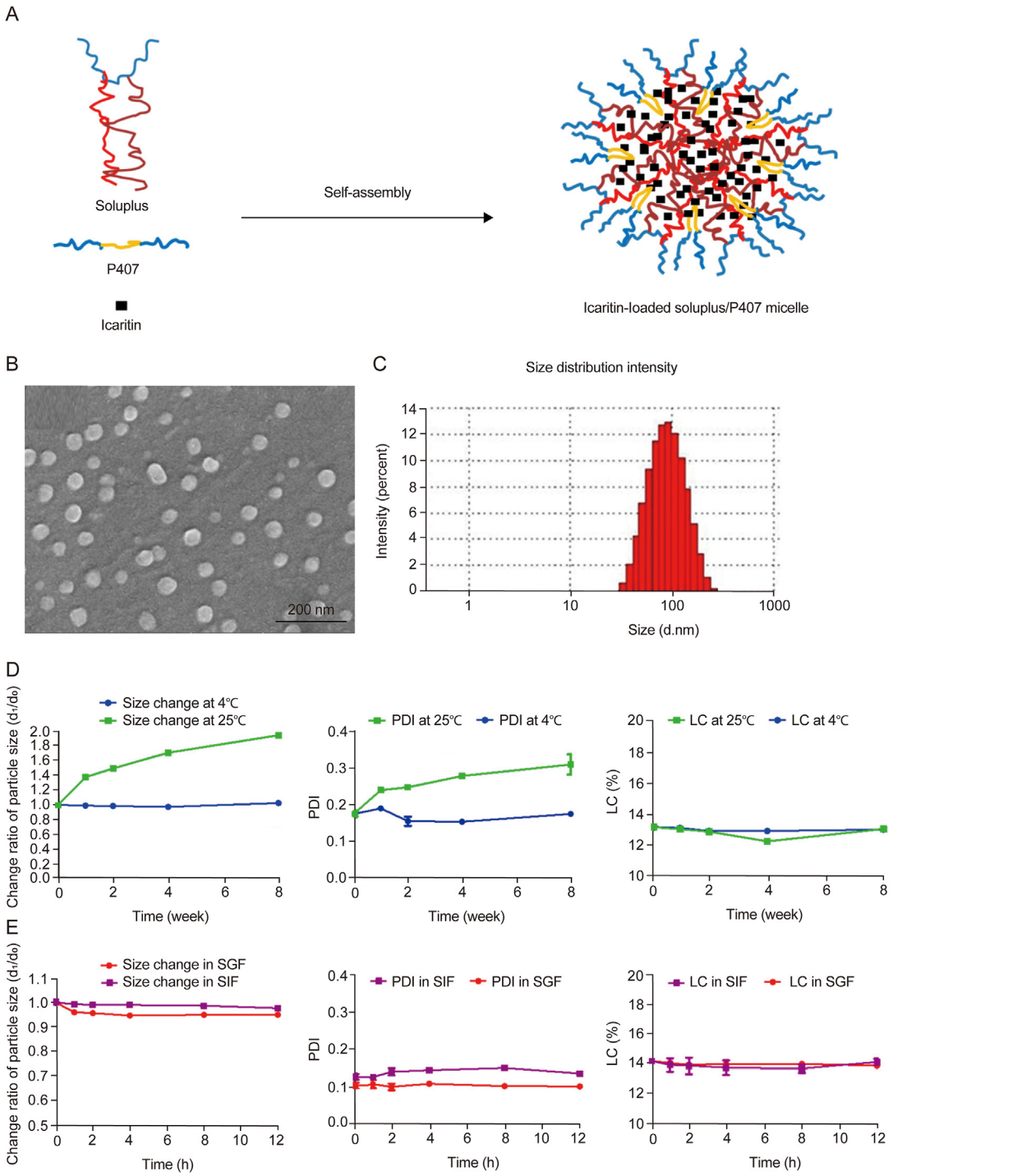

Fig. 5. The preparation, size, and high stability of icaritin-loaded polymeric micelles. (A) Diagram of the preparation of icaritin-loaded Soluplus®/Poloxamer 407 (P407) micelles by the acid-base shift method. (B) Scanning electron microscope (SEM) images of IPMs. (C) Size distribution of IPMs. (D, E) Changes in particle size, PDI and icaritin loading content of IPMs during storage at 4 °C and 25 °C (D), as well as upon a 25-fold dilution with SGF and SIF at 37 °C (E). Reprinted from Ref. [115] with permission. IPMs: icaritin-loaded polymeric micelles; PDI: polydispersity index; LC: loading content; SGF: simulated gastric fluid; SIF: simulated intestinal fluid.

Although PEG modification can prolong the blood circulation of NPs, this strategy is a double-edged sword that limits subsequent tumor penetration and cellular internalization. Other methods have also been proposed to prolong the blood circulation of NPs, such as surface decoration with the marker CD47 and hitchhiking of NPs on red blood cells (RBCs) [123,129]. The phagocytosis of NPs by RES can be prevented by coating NPs with CD47, an integrin-associated protein and a self-recognition marker on RBCs. In addition, RBCs have been proposed as carriers for drug-loaded NPs due to their diverse advantages of high biocompatibility, excellent homogeneity, and long circulation time. In the future, with the aim of expanding the applications of this novel drug delivery system,

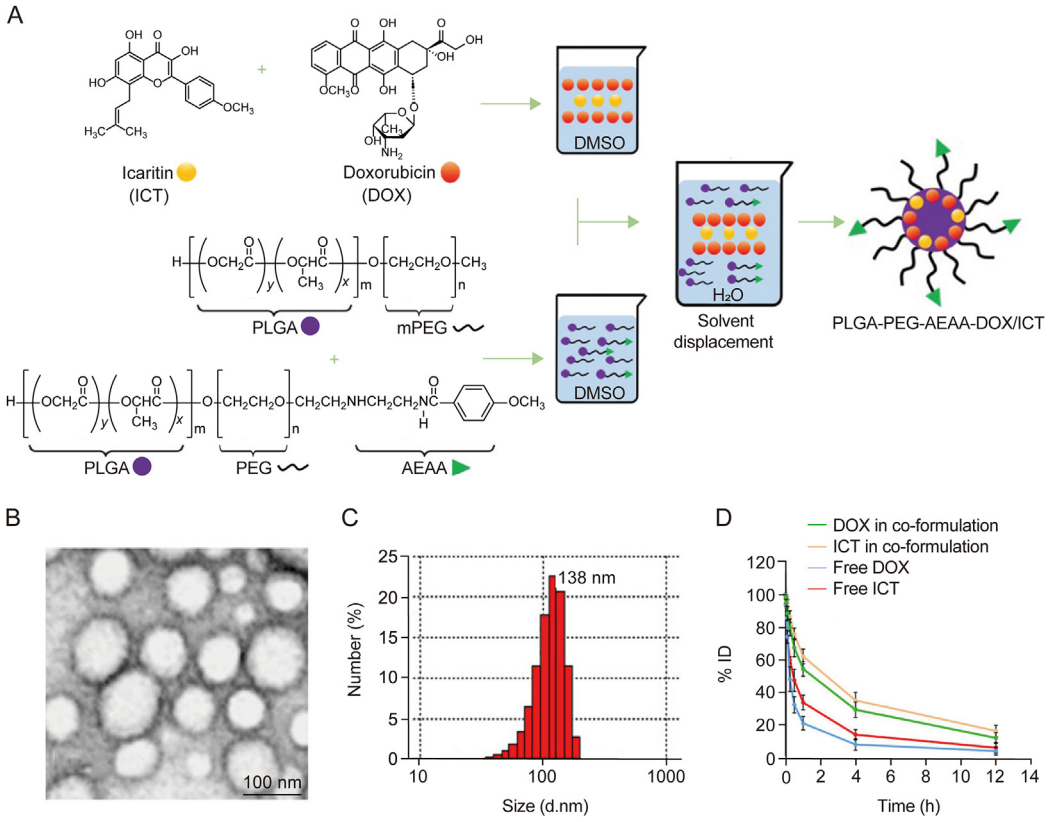

Fig. 6. Prolonged blood circulation of DOX/icaritin-loaded PLGA-PEG-AEAA NPs. (A) Efficient coencapsulation of icaritin and DOX into PLGA-PEG-AEAA NPs using a solvent displacement technique. (B) Transmission electron microscopy (TEM) images of DOX/icaritin coformulated NPs. (C) Particle size of the DOX/icaritin coformulated NPs. (D) Changes in icaritin (1 mg/kg) and DOX (3 mg/kg) coformulated NP concentrations after a single i.v. injection through the tail vein of mice ($n = 4$). Reprinted from Ref. [57] with permission. ICT: icaritin; DOX: doxorubicin; DMSO: dimethyl sulfoxide; PLGA: poly(lactic-*co*-glycolic acid); PEG: polyethylene glycol; mPEG: monomethoxy polyethylene glycol; AEAA: aminoethyl anisamide; NP: nanoparticle.

optimization of the size, shape, deformability, surface charge, and other features interfering with the interaction of NPs with RBCs is needed.

4.5. Augmented targeted accumulation

Delivery of drugs at high concentrations to the right target is required. NPs are endowed with the capacity to deliver drugs to target tissues, cells, and even organelles either passively or actively.

4.5.1. Passive targeting

NPs are so small that they cross the leaky blood-tumor barrier and accumulate in the tumor sites via a poor lymphatic system, which prevents the drainage of the intratumoral components. Such phenomenon is termed as the enhanced permeability and retention (EPR) effect [130]. The EPR effect of NPs has been widely utilized to improve drug delivery for cancer treatment. In our previous work, baohuoside I-loaded mixed micelles with lecithin and Solutol HS 15 (BLSM) were formed using a thin film hydration method, and their target behavior was evaluated [131]. The BSLM had a size of approximately 62.54 nm. The distribution of BLSM in lung tumor sites was clearly observed and maintained for 24 h, indicating the in vivo targeting of mixed micelles. As a result, the micelles exhibited remarkable antitumor effects, as evidenced by inhibited tumor growth. Although the EPR effect has been shown to be the important factor contributing to the improved therapeutic effects of nanoformulations, the EPR effect alone is insufficient due to its nonspecificity. In addition, the EPR effects are easily affected by various NP properties, such as size, shape, stiffness, and surface charge.

4.5.2. Active targeting

The use of targeting ligands, which is called active targeting, can further increase the targeted ability for specific tissues or cells, which is beyond the EPR effect [132–134]. For instance, Chen et al. [43] reported the successful application of an icaritin targeted delivery system in steroid-associated osteonecrosis (SAON). The eight repeating sequences of aspartate (Asp_8)-liposome-icaritin (ASP-LP-ICT) were prepared via the thin film evaporation method, as shown in Fig. S2A [43]. First, multilamellar vesicles were formed by thin film evaporation of methanol/chloroform organic solvent containing icaritin and lipids. The prepared liposome suspension was extruded to obtain small unilamellar vesicles. Then, moiety Asp_8 was utilized to modify the surface of liposomes and applied to anchor icaritin-loaded liposomes on bone-resorption surfaces because it prefers to bind with crystallized hydroxyapatite [135]. An in vivo distribution assay showed that ASP-LP could facilitate bone targeting and extend the retention time of icaritin in bone (Fig. S2B). Furthermore, ASP-LP-ICT effectively prevented steroid-treated rats from SAON with largely decreased osteocyte apoptosis, downregulated osteoclatsogenesis, and upregulated osteogenesis. The remarkable efficacy of ASP-LP-ICT benefited from the role of Asp8 in the accelerated target of icaritin on bone remodeling sites.

4.6. Elevated tumor penetration

Although NPs prolong blood circulation and augment targeted accumulation, they mainly accumulate at the periphery of tumor tissue due to the unique tumor microenvironment of the dense extracellular matrix (ECM) and interstitial fluid pressure (IFP), and NPs have difficulty in penetrating into the interior or distal end of the tumor [136]. This phenomenon explains why some extensively investigated anticancer nanomedicines, such as US Food and Drug Administration (US FDA)-approved Doxil and Abraxane, still show unsatisfactory clinical treatment [137]. To further improve therapeutic effects, it is important to develop nanomedicines with high tumor penetration capability.

Generally, the tumor penetration of nanomedicines can be improved by optimizing NP properties and modulating the tumor microenvironment [138]. As reported, several physical properties of NPs including size, shape, and charge, can be optimized to enhance tumor penetration. Smaller NPs can penetrate deeper into the tumor than large ones, while the size of NPs is also highly related to blood circulation and tumor accumulation [139]. Thus, the factors affecting NP fate in vivo should be taken into consideration in the design of nanomedicines. Additionally, compared with spherical NPs, nonspherical NPs have shown improved penetration due to their more complex dynamics and aspect ratios [140]. In terms of NP surface charge, cationic NPs show better penetrative ability [141]. Except for the properties of NPs, the complex tumor microenvironment mainly contributes to the poor penetration of nanomedicines. To strengthen the tumor penetration of nanomedicines, the tumor microenvironment can be adjusted through vascular disruption, vascular normalization, and ECM modulation [142]. One example of enhanced HCC tumor penetration of icaritin and coix seed oil-coloaded lipid complexes (IC-ML) was reported by Guo et al. [20]. As shown in Fig. 7A, during the preparation of IC-ML, icaritin and coix seed oil were first coloaded into microemulsions to form icaritin and coix seed oil co-loaded microemulsions (IC-MEs) [20]. Then the IC-MEs were encapsulated into thermosensitive liposomes to form IC-ML. IC-ML remained stable before delivery to the liver tumor and released the drug when mild hyperthermia (42 °C) was applied to the tumor site. The tumor penetration of various NPs on cancer-associated fibroblasts (CAFs) + tumor cells cocultured 3D tumor spheres was investigated (Fig. 7B). In contrast to microemulsions (MEs), ML and liposomes (L) showed enhanced tumor penetration at 320 μm. Owing to the higher penetration capability of ML and IC-ML, IC-ML incubated at 42 °C (H+) significantly inhibited the growth of tumor spheres and the mean area of tumor spheres was 1.640×10^5 μm^2, which was less than that of the tumor spheres treated with IC (3.240×10^5 μm^2), IC-MEs (2.110×10^5 μm^2), and IC-ML incubated at 37 °C (H−) (2.539×10^5 μm^2), indicating the improved antiproliferation effect of IC-ML (H+) on 3D tumor spheroids (Figs. 7C and D). Additionally, the in vivo distribution study also revealed that ML exhibited deeper tumor penetration than ME (Figs. 7E and F).

Although the two traditional strategies mentioned above can augment the tumor penetration of nanomedicines, there are some disadvantages. The method of modulating the tumor microenvironment affects later drug administration, and external physical forces, such as hyperthermia and ultrasound, are needed to be applied [138]. On the other hand, changing physical properties can have some adverse effects on delivery cascades. For instance, smaller NPs show enhanced tumor penetration, but they cannot be used due to their short half-life in blood circulation. To overcome these disadvantages, some novel strategies have been proposed, including transcellular transport of NPs and application of transformable NPs. Because the ECM hinders the NP paracellular transport in tumors, transcellular transport of NPs with penetration-assisted ligands can be an alternative to enhance tumor penetration [143]. In addition, transformable NPs, such as shrinkable size or reversible charge, can be utilized to meet the requirements during circulation, accumulation, and penetration simultaneously [138]. For example, during circulation, larger or negatively charged NPs accumulated at the tumor sites. With stimulation by UV light or pH, the size of the NPs will be reduced or surface charge will be reversed to positive charge, which results in the better penetration of the transformed NPs [144,145].

4.7. Overcoming multidrug resistance

Generally, tumors form resistance to one kind of anticancer drugs with repeated treatment and then become resistant to similar or completely different drugs, which is known as MDR [146]. Clinical applications of baohuoside I are significantly restricted due to the severe MDR caused by efflux of baohuoside I via ATP-binding cassette families such as *P*-glycoprotein (*P*-gp) and breast cancer resistance protein (BCRP) from cancer cells [120]. NPs can improve MDR reversing of baohuoside I and thereby extend its application.

NPs were reported to improve the permeability and inhibit efflux of baohuoside I by suppressing the *P*-gp efflux system. For example, our group compared the transport of baohuoside I and baohuoside I loaded mixed micelles composed of Solutol HS15 and Pluronic F127, which was prepared by the solvent evaporation method [120]. They found that the efflux of baohuoside I can be reduced by 316% with mixed micelles, indicating the *P*-gp efflux can be remarkably inhibited.

Besides, TPGS-based mixed micelles (Icar-MC) were produced using an anhydrous cosolvent reduction vaporization method by our group to deliver baohuoside I (icariside II) and explore their potential in the treatment of multidrug-resistant breast cancer [111]. In addition to improving the solubility of drugs, TPGS can also serve as a *P*-gp inhibitor and has been verified to improve the cytotoxicity of various drugs, such as DOX and paclitaxel [147]. The relative fluorescence value for retention of calcein acetoxymethyl ester (calcein AM) in TPGS micelle-treated MCF-7/ADR cells (122.3 ± 12.8) was higher than that in control (69.5 ± 1.8) and empty micelles (113.4 ± 11.5), indicating the robust inhibitory effects of TPGS on *P*-gp activity [111]. Owing to the *P*-gp inhibitory effect of TPGS and thereby improved accumulation of baohuoside I in the cells, Icar-MC displayed higher cytotoxicity than the free drug, as concluded by a lower IC_{50} (1.5-fold less than the free drug after 48 h of incubation) and a greater number of apoptotic cells (Figs. S3A and B). Furthermore, Icar-MC exhibited a stronger inhibitory effect on the proliferation of MCF-7/ADR cells and higher antitumor activity of Icar-MC than baohuoside I (Figs. S3C and D).

Overall, NPs can be applied as smart carriers to efficiently transfer active icaritin and baohuoside I to target tumor regions. With the assistance of nanotechnology, the bioavailability and delivery efficiency of icaritin and baohuoside I can be improved through various aspects, including drug stability, solubility, and permeability, blood circulation, targeting accumulation, tumor penetration, and MDR, thus enhancing the therapeutic effects. Nevertheless, NPs still have limitations of systemic immunogenicity, and some strategies, such as surface decoration of NPs with various zwitterionic ligands, coating NPs with cell membranes, and utilizing living cell delivery systems, could address these limitations and further improve the in vivo delivery efficiency of icaritin [148–150].

5. Applications of baohuoside I/icaritin-loaded NPs

Taking advantage of nanotechnology in drug in vivo delivery, baohuoside I or icaritin-loaded NPs can be used to improve the

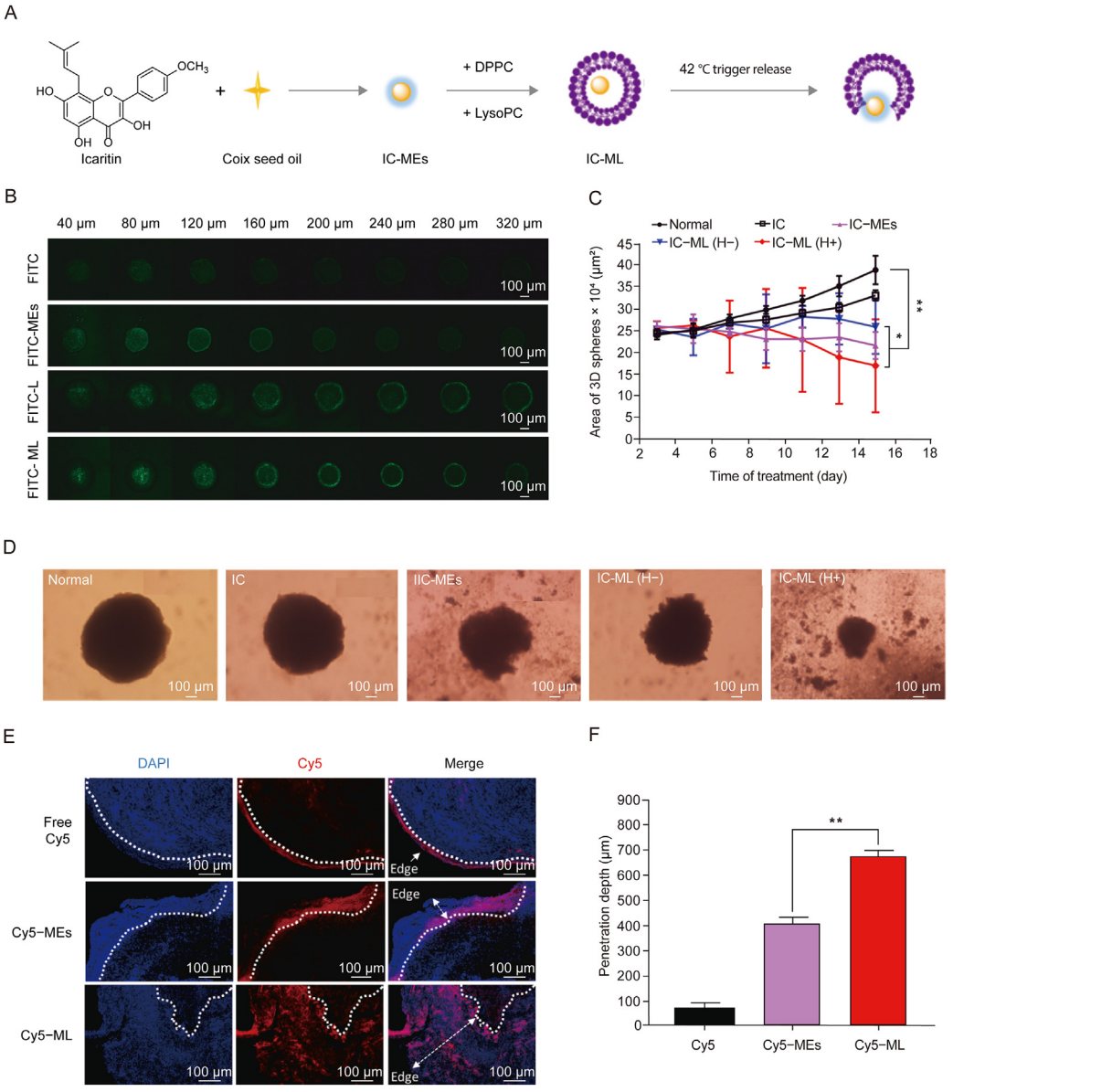

Fig. 7. Enhanced tumor penetration of icaritin and coix seed oil-coloaded lipid complexes. (A) Schematic illustration of icaritin and coix seed oil coloaded multicomponent thermosensitive lipid complexes. (B) Penetration evaluation of different formulations in HepG2+LX-2 cocultured 3D tumor spheroids. (C) Anti-proliferation effect of different formulations against 3D tumor spheres. $^{*}P < 0.05$, $^{**}P < 0.01$. (D) Appearance of 3D tumor spheres treated with various formulations by light microscope. (E) Immunofluorescence of tumor tissues treated with several formulation groups. Blue indicates the nucleus stained by DAPI, and the red indicates the various Cy5-labled formulations. (F) Penetration depth of several formulations in mouse tumors. $^{**}P < 0.01$. Reprinted from Ref. [20] with permission. DPPC: 1,2-dipalmitoyl-sn-glycero-3-phosphatidylcholine; LysoPC: lysophosphatidylcholine from soybean; FITC: fluorescein isothiocyanate; FITC-MEs: FITC-labeled microemulsions; FITC-L: FITC-labelled liposomes; FITC-ML: FITC-labeled ML; IC: icaritin; IC-MEs: icaritin and coix seed oil co-loaded microemulsions; IC-ML: icaritin and coix seed oil-coloaded lipid complexes; IC-ML (H+): IC-ML incubated at 42 °C; IC-ML (H−): IC-ML incubated at 37 °C; DAPI: 4′,6-diamidino-2-phenylindole.

treatment of various diseases with low side effects, such as cancers and osteonecrosis.

5.1. Cancer treatment

Numerous studies have shown that baohuoside I and icaritin have anticancer activities. As chemotherapeutic agents, baohuoside I and icaritin exert their therapeutic effects through tumor cell apoptosis and cell cycle arrest induction, autophagy triggering, cancer cell metastasis inhibition, and angiogenesis inhibition [151,152]. Many kinds of baohuoside I- or icaritin-loaded NPs have been applied to treat various cancers, such as breast cancer and lung cancer [35,57,111]. For instance, baohuoside I-encapsulated mixed micelles, consisting of TPGS and phospholipids, displayed stronger anticancer effects than free baohuoside I due to the MDR inhibition and could be a favorable delivery system to treat multi-drug-resistant breast cancer [111].

Notably, icaritin was found to modulate the immune system and can be utilized in immunotherapy. In a study of immune-based therapy for HCC, icaritin was demonstrated to induce both mitophagy and apoptosis and subsequently activate immunogenic cell death (ICD) biomarkers in HCC cells (Fig. 8A) [57]. Icaritin and DOX were coloaded into PLGA-PEG-AEAA NPs (combo NPs) and their immune-based therapeutic effects were investigated. Combo NPs displayed enhanced tumor growth inhibition compared with phosphate buffered saline (PBS)-, blank NP-, and either icaritin- or

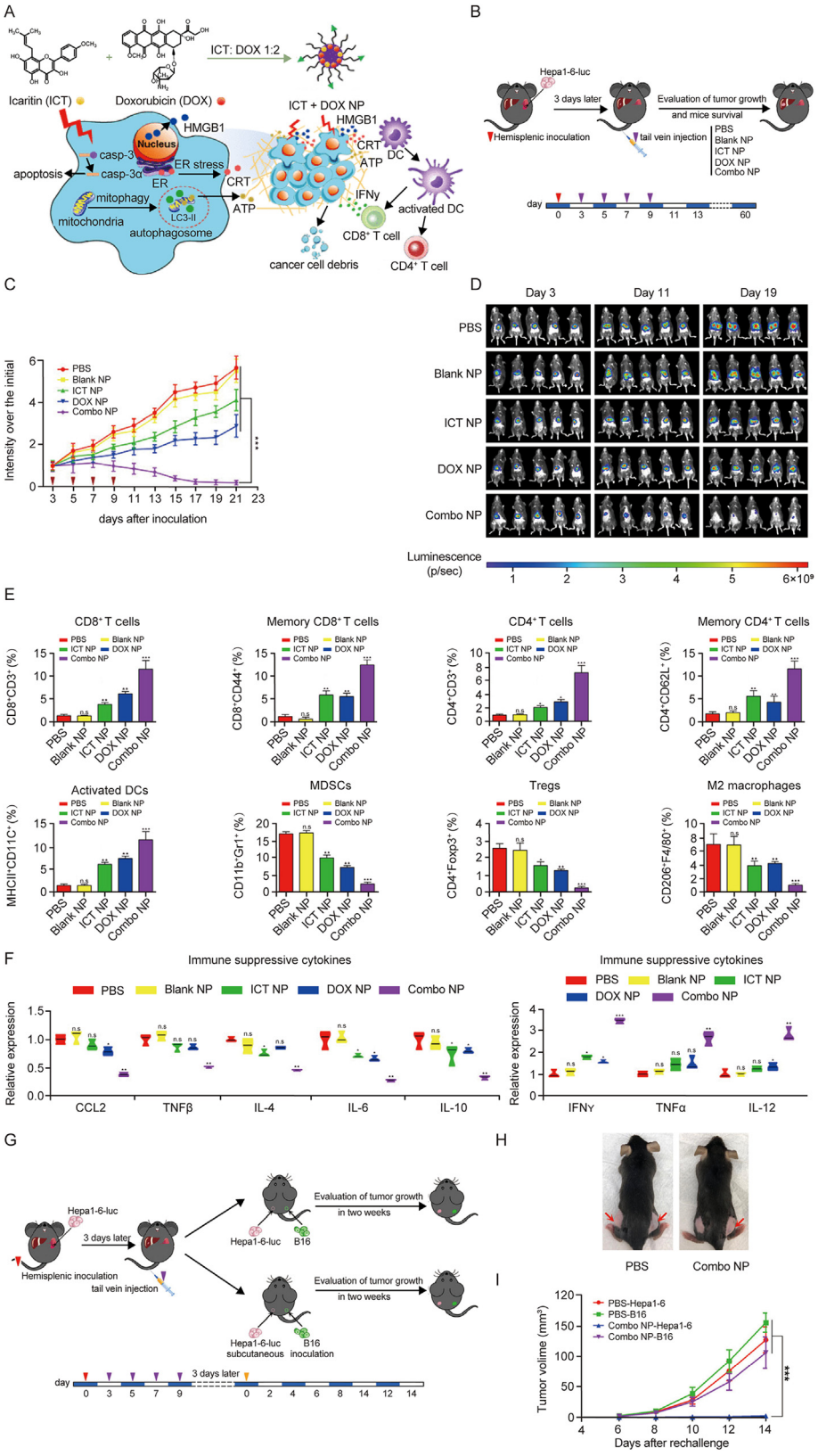

Fig. 8. Application of icaritin and DOX-coloaded PLGA-PEG-AEAA NPs (combo NPs) in HCC treatment. (A) ICD induced by combo NPs. Combo NPs could inhibit HCC by increasing the release of damage-associated molecular patterns (i.e., CRT, ATP, and HMGB1), immunosurveillance cells (i.e., $CD8^+$ T cells, $CD4^+$ T cells, and activated DC cells), and the immunostimulatory cytokines (i.e., IFN-γ, TNF-α, and IL-12). (B–F) Immune microenvironment remodeling of combo NPs: (B) tumor inoculation and treatment timeline; (C) tumor growth curve with treatments using various formulations; (D) Hepa1–6 tumor-bearing mice bioluminescence imaging with various treatments; (E) immunosurveillance cells (i.e., $CD8^+$ T cells, $CD4^+$ T cells, and activated DC cells), and immunosuppressive cells (i.e., MDSC, Treg, and M2) detected by flow cytometry; (F) expression of chemokines and cytokines detected by real-time PCR. (G, H, I) Antitumor vaccination effect of combo NPs: (G) tumor inoculation and treatment timeline; (H) image of Hepa1–6 and B16 tumor bearing mice (on the left and right side of mice respectively) treated with PBS (left) and combo NPs (right); (I) tumor growth curves with treatments using various formulations. Reprinted from

DOX-loaded NP-treated groups (Figs. 8B–D). To verify the ICD effect of combo NPs, changes in the release of damage-associated molecular patterns were detected. Increased release of the ICD markers CRT and HMGB1 was found in the Hepa 1–6-Luc HCC model treated with icaritin and DOX coencapsulated NPs (combo NPs). In addition, upregulated immunosurveillance cells, downregulated immunosuppressive cells, and increased immunostimulatory cytokines were observed in combo NP group, indicating that combo NPs could remodel the immune microenvironment to suppress HCC development (Figs. 8E–G). Furthermore, an antitumor vaccination effect of combo NPs on Hepa1–6 tumors, but not on B16 murine melanoma, was detected (Figs. 8H and I).

5.2. Osteonecrosis treatment

Baohuoside I and icaritin exert anti-osteonecrosis effects by inhibiting both thrombosis and lipid deposition [43]. Recently, baohuoside I- and icaritin-loaded NPs have been reported to treat osteonecrosis. For example, the effective NPs (ASP-LP-ICT) were developed to prevent osteonecrosis, and the mechanism behind accelerated osteogenesis promotion was investigated [43]. Owing to the prolonged circulation time of icaritin and bone target delivery by Asp8, ASP-LP-ICT showed inhibitory activity toward osteonecrosis in terms of reducing osteoclasts, enhancing osteoblastogenesis and formation, suppressing lipid deposition, and reducing inflammatory factors and cell apoptosis. As shown in Fig. S4A, the amount and erosion activity of osteoclasts were decreased by ASP-LP-ICT [43]. The improved bone formation was verified by the apparent wider distance between double-labeled fluorescent lines and increased osteogenic markers such as *Runx 2*, *Sp7*, and *Bglap* (Fig. S4B). Additionally, ASP-LP-ICT displayed an inhibitory effect on lipid deposition and downregulation of *Ppary* expression (Fig. S4C). Release of the inflammatory factors such as tumor necrosis factor alpha (TNF-α) and interleukin-1 beta (IL-1β), and cell apoptosis were also reduced by ASP-LP-ICT (Fig. S4D).

Overall, a large number of preclinical studies have already shown that the application of baohuoside I or icaritin-based nanomedicines can boost their therapeutic efficacy in various diseases. Clinical translation of these nanomedicines is urgently needed. Until 2021, there were 15 systemically administered anticancer nanomedicines that have been approved for clinical use and more than 50 nanomedicines against cancers are undergoing clinical trials [153,154]. According to the outcomes of clinical trials, these anticancer nanomedicines exhibit improved pharmacokinetics, enhanced antitumor efficacy, and reduced side effects over free drugs. For instance, Doxil, the nanomedicine approved for treating ovarian cancer and Kaposi's sarcoma, can significantly decrease the cardiotoxicity of the free drug DOX [153,155]. The approved anticancer nanomedicines encourage the clinical translation of baohuoside I or icaritin-based nanomedicines. Prolonged overall survival, an increased overall response rate, and reduced systemic toxicity can be achieved by baohuoside I or icaritin-based nanomedicines during clinical application in various diseases.

6. Conclusions and future perspectives

In summary, baohuoside I and icaritin are the major active flavonoids in EF and possess excellent therapeutic effects on various diseases. Specially, icaritin can be used in chemotherapy and also shows immune-modulating effects on cancer cells. With the aim of increasing productivity and activity, improving delivery efficiency in vivo, and enhancing the therapeutic effects of baohuoside I and icaritin, several strategies including production by enzymatic hydrolysis and delivery by NPs are summarized. NPs as drug delivery platforms can enhance the therapeutic effects of these active flavonoids by improving their stability and bioavailability, prolonging blood circulation, augmenting targeted accumulation, elevating tumor penetration, and overcoming MDR.

Although these strategies show accelerated production efficiency, delivery effects, and therapeutic efficacy, some challenges need to be addressed. First, the SAR of flavonoids derived from EF should be completely revealed, which will advance the exploration of derivatives of baohuoside I or icaritin with higher therapeutic effects.

Second, the productivity of baohuoside I and icaritin decreases when enzyme activity and stability are impaired during long-term reactions. Seeking for highly stable enzymes that can withstand high reaction temperatures, product inhibition, and organic solvents would be a good option. Additionally, to further simplify operation procedures and improve the enzyme recycling efficiency, additional enzyme immobilization materials can be used for enzyme immobilization. In terms of preparing baohuoside I and icaritin in a biphase enzymatic hydrolysis system, organic solvents can be replaced with certain noninvasive green solvents. Moreover, the combination of these approaches has the potential possibility of increasing the productivity of baohuoside I or icaritin and accelerating its application in industrial large-scale production.

Third, the clinical usage of these nanomedicines is limited because of the cytotoxicity and immunogenicity of NPs. Utilizing some kinds of bionic or live delivery vehicles in the transport of baohuoside I and icaritin would be an ideal solution to alleviate the cytotoxicity and immunogenicity.

Fourth, although enhanced therapeutic effects have been achieved with baohuoside I or icaritin-loaded NPs, they are still far away from clinical application. The in vivo behavior of nanomedicine interferes with the complex biological environment, and thus, the administration of baohuoside I or icaritin nanoformulations should be monitored throughout the delivery cascade, including blood circulation, tumor accumulation, penetration, tumor cell internalization, and finally the release of drugs in cells rather than only part of it. The in vivo toxicity, delivery efficiency, and therapeutic efficacy of these nanomedicines should be investigated comprehensively. In this way, nanomedicines with enhanced therapeutic effects are more likely to be applied in clinical treatments. Additionally, investigations of baohuoside I- or icaritin loaded NPs for the treatment of other diseases such as cardiovascular diseases and sexual dysfunction can be further implemented.

In summary, baohuoside I and icaritin possess various therapeutic effects and merit further exploration of their role in disease prevention and therapy. In terms of their low content in natural plants and inferior bioavailability, efforts to optimize enzymatic hydrolysis methods of preparation and smart NP-based delivery systems have been exerted to improve therapeutic effects. Inspired by the 15 anticancer nanomedicines approved for clinical use, the clinical translation of baohuoside I or icaritin-loaded NPs would benefit patients. We are convinced that with rational design and continuing studies, a bright future can be foreseen for effective treatment of these bioactive flavonoids in various human diseases.

Ref. [57] with permission. NP: nanoparticle; ICD: immunogenic cell death; HCC: hepatocellular carcinoma; PLGA: poly (lactic-*co*-glycolic acid); PEG: polyethylene glycol; mPEG: monomethoxy polyethylene glycol; AEAA: aminoethyl anisamide; ICT: icaritin; DOX: doxorubicin; HMGB1: high mobility group box 1; ER: estrogen receptor; CRT: calreticulin; ATP: adenosine triphosphate; LC3-II: microtubule-associated protein light chain 3 II; DC: dendritic cell; CCL2: C–C motif chemokine ligand 2; TGF-β: transforming growth factor beta; IL-4: interleukin-4; IFN-γ: interferon gamma; TNF-α: tumor necrosis factor alpha; MDSCs: myeloid-derived suppressor cells; Tregs: regulatory T cells; PBS: phosphate buffered saline. $^{*}P < 0.05$, $^{**}P < 0.01$, $^{***}P < 0.001$, n.s: no significance.

CRediT author statement

Yi Lu: Investigation, Writing - Original draft preparation; **Qiulan Luo:** Funding acquisition, Writing - Reviewing and Editing; **Xiaobin Jia:** Methodology; **James P. Tam:** Methodology; **Huan Yang:** Conceptualization, Project administration, Writing - Reviewing and Editing; **Yuping Shen:** Supervision, Funding acquisition, Writing - Reviewing and Editing; **Xin Li:** Conceptualization, Project administration, Supervision, Writing - Reviewing and Editing.

Declaration of competing interest

The authors declare that there are no conflicts of interest.

Acknowledgments

This work was supported by the National Natural Science Foundation of China (Grant No.: 81873196), Sino-German Center for Research Promotion (Project No.: GZ1505), Chinese Scholarship Council, and Science and Technology Planning Projects of Jiaxing City (Project No.: 2022AY10014).

Appendix A. Supplementary data

Supplementary data to this article can be found online at https://doi.org/10.1016/j.jpha.2022.12.001.

References

[1] H.P. Ma, X.R. He, Y. Yang, et al., The genus epimedium: An ethnopharmacological and phytochemical review, J. Ethnopharmacol. 134 (2011) 519–541.
[2] C.P. Commission, Pharmacopoeia of the People's Republic of China. Vol. 1, China Medical Science Press, Beijing, 2015.
[3] X.D. Su, W. Li, J.Y. Ma, et al., Chemical constituents from *Epimedium koreanum* nakai and their chemotaxonomic significance, Nat. Prod. Res. 32 (2018) 2347–2351.
[4] Y. Shen, M. Wang, Y. Chen, et al., Convenient preparation of sagittatoside B, a rare bioactive secondary flavonol glycoside, by recyclable and integrated biphase enzymatic hydrolysis, Enzym. Microb. Technol. 121 (2019) 51–58.
[5] T. Cheng, Y. Zhang, T. Zhang, et al., Comparative pharmacokinetics study of icariin and icariside II in rats, Molecules 20 (2015) 21274–21286.
[6] X. Cao, Q. Luo, F. Song, et al., Effects of oxidative torrefaction on the physicochemical properties and pyrolysis products of hemicellulose in bamboo processing residues, Ind. Crop. Prod. 191 (2023), 115986.
[7] H. Wu, M. Kim, J. Han, Icariin metabolism by human intestinal microflora, Molecules 21 (2016), 1158.
[8] Y. Li, S. Sun, Q. Chang, et al., A strategy for the improvement of the bioavailability and antiosteoporosis activity of BCS IV flavonoid glycosides through the formulation of their lipophilic aglycone into nanocrystals, Mol. Pharm. 10 (2013) 2534–2542.
[9] Y. Lu, Y. Gao, H. Yang, et al., Nanomedicine-boosting icaritin-based immunotherapy of advanced hepatocellular carcinoma, Mil. Med. Res. 9 (2022), 69.
[10] Y. Sun, S. Qin, W. Li, et al., A randomized, double-blinded, phase III study of icaritin versus huachashu as the first-line therapy in biomarker-enriched HBV-related advanced hepatocellular carcinoma with poor conditions: Interim analysis result, J. Clin. Oncol. 39 (2021), S4077.
[11] S. Lu, K. Zou, B. Guo, et al., One-step purification and immobilization of thermostable β-glucosidase on na-y zeolite based on the linker and its application in the efficient production of baohuoside I from icariin, Bioorg. Chem. 121 (2022), 105690.
[12] F. Liu, B. Wei, L. Cheng, et al., Co-immobilizing two glycosidases based on cross-linked enzyme aggregates to enhance enzymatic properties for achieving high titer icaritin biosynthesis, J. Agric. Food Chem. 70 (2022) 11631–11642.
[13] X. Jin, Z.H. Zhang, E. Sun, et al., A novel drug–phospholipid complex loaded micelle for baohuoside I enhanced oral absorption: *In vivo* and *in vivo* evaluations, Drug Dev. Ind. Pharm. 39 (2013) 1421–1430.
[14] L. Huang, X. Wang, H. Cao, et al., A bone-targeting delivery system carrying osteogenic phytomolecule icaritin prevents osteoporosis in mice, Biomaterials 182 (2018) 58–71.
[15] X. Chen, H. Ji, Q. Zhang, et al., A rapid method for simultaneous determination of 15 flavonoids in *Epimedium* using pressurized liquid extraction and ultra-performance liquid chromatography, J. Pharm. Biomed. Anal. 46 (2008) 226–235.
[16] J. Tong, C. Liu, B. Wang, Improved synthesis of icaritin and total synthesis of β-anhydroicaritin, Chem. Res. Chin. Univ. 35 (2019) 616–620.
[17] J. Xie, J. Zhao, N. Zhang, et al., Efficient production of isoquercitin, icariin and icariside II by a novel thermostable α-L-rhamnosidase PodoRha from Paenibacillus odorifer with high α-1, 6-/α-1, 2- glycoside specificity, Enzym. Microb. Technol. 158 (2022), 110039.
[18] H. Khan, H. Ullah, M. Martorell, et al., Flavonoids nanoparticles in cancer: Treatment, prevention and clinical prospects, Semin. Cancer Biol. 69 (2021) 200–211.
[19] J. Zhang, K. Hu, L. Di, et al., Traditional herbal medicine and nanomedicine: Converging disciplines to improve therapeutic efficacy and human health, Adv. Drug Deliv. Rev. 178 (2021), 113964.
[20] J. Guo, H. Zeng, Y. Liu, et al., Multicomponent thermosensitive lipid complexes enhance desmoplastic tumor therapy through boosting antiangiogenesis and synergistic strategy, Int. J. Pharm. 601 (2021), 120533.
[21] X. Li, Y. Lu, Y. Hu, A wireless and battery-free DNA hydrogel biosensor for wound infection monitoring, Matter 5 (2022) 2473–2475.
[22] T.Y. Wang, Q. Li, K.S. Bi, Bioactive flavonoids in medicinal plants: Structure, activity and biological fate, Asian J. Pharm. Sci. 13 (2018) 12–23.
[23] S. Shi, J. Li, X. Zhao, et al., A comprehensive review: Biological activity, modification and synthetic methodologies of prenylated flavonoids, Phytochemistry 191 (2021), 112895.
[24] Y.H. Xi, T.W. Jiang, J.M. Yu, et al., Preliminary studies on the anti-osteoporosis activity of baohuoside I, Biomed. Pharmacother. 115 (2019), 108850.
[25] H.J. Choi, J.S. Eun, D.K. Kim, et al., Icariside II from *Epimedium* koreanum inhibits hypoxia-inducible factor-1 alpha in human osteosarcoma cells, Eur. J. Pharmacol. 579 (2008) 58–65.
[26] M.B. Liu, W. Wang, J.M. Gao, et al., Icariside II attenuates cerebral ischemia/reperfusion-induced blood–brain barrier dysfunction in rats via regulating the balance of MMP9/TIMP1, Acta Pharmacol. Sin. 41 (2020) 1547–1556.
[27] B.F. Guan, X.F. Dai, Q.B. Huang, et al., Icariside II ameliorates myocardial ischemia and reperfusion injury by attenuating inflammation and apoptosis through the regulation of the PI3K/AKT signaling pathway, Mol. Med. Rep. 22 (2020) 3151–3160.
[28] L. Yang, C. Peng, J. Xia, et al., Effects of icariside II ameliorates diabetic cardiomyopathy in streptozotocin-induced diabetic rats by activating Akt/NOS/NF-κB signaling, Mol. Med. Rep. 17 (2018) 4099–4105.
[29] S.j. Gu, M. Li, Y.m. Yuan, et al., A novel flavonoid derivative of icariside II improves erectile dysfunction in a rat model of cavernous nerve injury, Andrology 9 (2021) 1893–1901.
[30] L. Yan, Y. Deng, J. Gao, et al., Icariside II effectively reduces spatial learning and memory impairments in Alzheimer's disease model mice targeting beta-amyloid production, Front. Pharmacol. 8 (2017), 106.
[31] J. Zhou, Y. Deng, F. Li, et al., Icariside II attenuates lipopolysaccharide-induced neuroinflammation through inhibiting TLR4/MYD88/NF-κB pathway in rats, Biomed. Pharmacother. 111 (2019) 315–324.
[32] C. Tian, F. Gao, X. Li, et al., Icariside ii attenuates eosinophils-induced airway inflammation and remodeling via inactivation of NF-κB and STAT3 in an asthma mouse model, Exp. Mol. Pathol. 113 (2020), 104373.
[33] Y. Chen, L.N. Zhang, X.Y. Zang, et al., Baohuoside I inhibits tumor angiogenesis in multiple myeloma via the peroxisome proliferator-activated receptor gamma/vascular endothelial growth factor signaling pathway, Front. Pharmacol. 13 (2022), 822082.
[34] K.S. Lee, H.J. Lee, K.S. Ahn, et al., Cyclooxygenase-2/prostaglandin e-2 pathway mediates icariside II induced apoptosis in human pc-3 prostate cancer cells, Cancer Lett. 280 (2009) 93–100.
[35] H.M. Yan, J. Song, X.B. Jia, et al., Hyaluronic acid-modified didecyldimethylammonium bromide/d-a-tocopheryl polyethylene glycol succinate mixed micelles for delivery of baohuoside I against non-small cell lung cancer: *In vitro* and *in vivo* evaluation, Drug Deliv. 24 (2017) 30–39.
[36] Y.S. Sun, K. Thakur, F. Hu, et al., Icariside II suppresses cervical cancer cell migration through JNK modulated matrix metalloproteinase-2/9 inhibition *in vitro* and *in vivo*, Biomed. Pharmacother. 125 (2020), 110013.
[37] S. Wang, N. Wang, X. Huang, et al., Baohuoside I suppresses breast cancer metastasis by downregulating the tumor-associated macrophages/cxc motif chemokine ligand 1 pathway, Phytomedicine 78 (2020), 153331.
[38] F. Ni, H. Tang, C. Wang, et al., Baohuoside I inhibits the proliferation of pancreatic cancer cells via mTOR/S6K1-caspases/Bcl2/Bax apoptotic signaling, Cancer Manag. Res. 11 (2019) 10609–10621.
[39] Y. Guo, H. Zhu, M. Weng, et al., Baohuoside-1 targeting mTOR inducing apoptsis to inhibit hepatocellular carcinoma proliferation, invasion and migration, Biomed. Pharmacother. 128 (2020), 110366.
[40] Q. Wang, S. Jiang, W. Wang, et al., Effects of baohuoside-I on epithelial-mesenchymal transition and metastasis in nasopharyngeal carcinoma, Hum. Exp. Toxicol. 40 (2021) 566–576.
[41] Y. Guo, C. Wang, M. Jiang, et al., Baohuoside I via mtor apoptotic signaling to inhibit glioma cell growth, Cancer Manag. Res. 12 (2020) 11435–11444.
[42] Y.G. Peng, L. Zhang, Baohuoside-I suppresses cell proliferation and migration by up-regulating mir-144 in melanoma, Pharm. Biol. 56 (2017) 43–50.
[43] S. Chen, L. Zheng, J. Zhang, et al., A novel bone targeting delivery system carrying phytomolecule icaritin for prevention of steroid-associated osteonecrosis in rats, Bone 106 (2018) 52–60.
[44] W. Zhang, B. Xing, L. Yang, et al., Icaritin attenuates myocardial ischemia and reperfusion injury via anti-inflammatory and anti-oxidative stress effects in rats, Am. J. Chin. Med. 43 (2015) 1083–1097.

[45] S. Zhu, Z. Wang, Z. Li, et al., Icaritin suppresses multiple myeloma, by inhibiting IL-6/JAK2/STAT3, Oncotarget 6 (2015) 10460–10472.
[46] J. Li, P. Liu, R. Zhang, et al., Icaritin induces cell death in activated hepatic stellate cells through mitochondrial activated apoptosis and ameliorates the development of liver fibrosis in rats, J. Ethnopharmacol. 137 (2011) 714–723.
[47] L. Liu, Z. Zhao, L. Lu, et al., Icariin and icaritin ameliorated hippocampus neuroinflammation via mediating hmgb1 expression in social defeat model in mice, Int. Immunopharm. 75 (2019), 105799.
[48] H. Wu, X. Liu, Z.Y. Gao, et al., Icaritin provides neuroprotection in Parkinson's disease by attenuating neuroinflammation, oxidative stress, and energy deficiency, Antioxidants 10 (2021) 529.
[49] X. Chen, L. Song, Y. Hou, et al., Reactive oxygen species induced by icaritin promote DNA strand breaks and apoptosis in human cervical cancer cells, Oncol. Rep. 41 (2019) 765–778.
[50] L. Yin, X.W. Qi, X.Z. Liu, et al., Icaritin enhances the efficacy of cetuximab against triple-negative breast cancer cells, Oncol. Lett. 19 (2020) 3950–3958.
[51] F. Sun, I.R. Indran, Z.W. Zhang, et al., A novel prostate cancer therapeutic strategy using icaritin-activated arylhydrocarbon-receptor to co-target androgen receptor and its splice variants, Carcinogenesis 36 (2015) 757–768.
[52] L. Gao, M. Chen, Y. Ouyang, et al., Icaritin induces ovarian cancer cell apoptosis through activation of p53 and inhibition of Akt/mTOR pathway, Life Sci. 202 (2018) 188–194.
[53] X.W. Pan, L. Li, Y. Huang, et al., Icaritin acts synergistically with epirubicin to suppress bladder cancer growth through inhibition of autophagy, Oncol. Rep. 35 (2016) 334–342.
[54] C. Zhou, Z. Chen, X. Lu, et al., Icaritin activates JNK-dependent mPTP necrosis pathway in colorectal cancer cells, Tumor Biol. 37 (2016) 3135–3144.
[55] Z. Li, X. Meng, L. Jin, Icaritin induces apoptotic and autophagic cell death in human glioblastoma cells, Am. J. Transl. Res. 8 (2016) 4628–4643.
[56] X.J. Yang, Y.M. Xi, Z.J. Li, Icaritin: a novel natural candidate for hematological malignancies therapy, BioMed Res. Int. 2019 (2019), 4860268.
[57] Z. Yu, J. Guo, M. Hu, et al., Icaritin exacerbates mitophagy and synergizes with doxorubicin to induce immunogenic cell death in hepatocellular carcinoma, ACS Nano 14 (2020) 4816–4828.
[58] Y.H. Tang, Y.F. Li, D.W. Xin, et al., Icariin alleviates osteoarthritis by regulating autophagy of chondrocytes by mediating PI3K/AKT/mTOR signaling, Bioengineered 12 (2021) 2984–2999.
[59] N. Liu, T. Zhang, B.R. Cao, et al., Icariin possesses chondroprotective efficacy in a rat model of dexamethasone-induced cartilage injury through the activation of miR-206 targeting of cathepsin k, Int. J. Mol. Med. 41 (2018) 1039–1047.
[60] X. Meng, H. Pei, C. Lan, Icariin exerts protective effect against myocardial ischemia/reperfusion injury in rats, Cell Biochem. Biophys. 73 (2015) 229–235.
[61] H.A. Chen, C.M. Chen, S.S. Guan, et al., The antifibrotic and anti-inflammatory effects of icariin on the kidney in a unilateral ureteral obstruction mouse model, Phytomedicine 59 (2019), 152917.
[62] X.L. Zhang, N.N. Han, G.Q. Li, et al., Local icariin application enhanced periodontal tissue regeneration and relieved local inflammation in a minipig model of periodontitis, Int. J. Oral Sci. 10 (2018) 19.
[63] J.W. Wang, G.S. Zhu, X.Y. Wang, et al., An injectable liposome for sustained release of icariin to the treatment of acute blunt muscle injury, J. Pharm. Pharmacol. 72 (2020) 1152–1164.
[64] X. Zheng, D.H. Li, J.X. Li, et al., Optimization of the process for purifying icariin from Herba Epimedii by macroporous resin and the regulatory role of icariin in the tumor immune microenvironment, Biomed. Pharmacother. 118 (2019), 109275.
[65] L. Song, X. Chen, L. Mi, et al., Icariin-induced inhibition of SIRT6/NF-κB triggers redox mediated apoptosis and enhances anti-tumor immunity in triple-negative breast cancer, Cancer Sci. 111 (2020) 4242–4256.
[66] N.A. Alhakamy, U.A. Fahmy, S.M. Badr-Eldin, et al., Optimized icariin phytosomes exhibit enhanced cytotoxicity and apoptosis-inducing activities in ovarian cancer cells, Pharmaceutics 12 (2020), 346.
[67] C.Y. Li, S.Q. Yang, H.Q. Ma, et al., Influence of icariin on inflammation, apoptosis, invasion, and tumor immunity in cervical cancer by reducing the TLR4/MyD88/NF-κB and Wnt/β-catenin pathways, Cancer Cell Int. 21 (2021), 206.
[68] J. Ding, Y. Tang, Z. Tang, et al., Icariin improves the sexual function of male mice through the PI3K/AKT/eNOS/NO signalling pathway, Andrologia 50 (2018), e12802.
[69] C.X. Sheng, P.P. Xu, K.X. Zhou, et al., Icariin attenuates synaptic and cognitive deficits in an A β_{1-42}-induced rat model of Alzheimer's disease, BioMed Res. Int. 2017 (2017), 7464872.
[70] Z. Wang, H. Zhang, L.L. Dai, et al., Arsenic trioxide and icariin show synergistic anti-leukemic activity, Cell Biochem. Biophys. 73 (2015) 213–219.
[71] R. Shen, W.J. Deng, C. Li, et al., A natural flavonoid glucoside icariin inhibits Th1 and Th17 cell differentiation and ameliorates experimental autoimmune encephalomyelitis, Int. Immunopharm. 24 (2015) 224–231.
[72] W. Xiong, H. Ma, Z. Zhang, et al., The protective effect of icariin and phosphorylated icariin against LPS-induced intestinal goblet cell dysfunction, Innate Immun. 26 (2020) 97–106.
[73] Y. Xie, L. Xie, A. Chen, et al., Anti-HIV/SIV activity of icariin and its metabolite anhydroicaritin mainly involve reverse transcriptase, Eur. J. Pharmacol. 884 (2020), 173327.
[74] X.J. Chen, Z.H. Tang, X.W. Li, et al., Chemical constituents, quality control, and bioactivity of epimedii folium (Yinyanghuo), Am. J. Chin. Med. 43 (2015) 783–834.
[75] Z.S. Xu, L.L. Huang, T.T. Sun, et al., Comparison of the total flavonoids content in epimedii folium processed by monlton suet from different growing areas and different positions of sheep or goat, Chin. J. Exp. Tradit. Med. Formulae 23 (2012) 149–152.
[76] X.B. Jia, X.Y. Jin, J.J. Wang, et al., Comparison of the content of main component in *epimedium koreanum* decoction pieces from different manufactories, Chin. Pharm. 21 (2010) 1006–1008.
[77] M. Dong, S.X. Wu, H.J. Xu, et al., Fbs-derived exosomes as a natural nanoscale carrier for icariin promote osteoblast proliferation, Front. Bioeng. Biotechnol. 9 (2021), 615920.
[78] Y. Liu, H. Yang, J. Xiong, et al., Icariin as an emerging candidate drug for anticancer treatment: current status and perspective, Biomed. Pharmacother. 157 (2023), 113991.
[79] Y.K. Zhai, B.F. Ge, K.M. Chen, et al., Comparative study on the osteogenic differentiation of rat bone marrow stromal cells effected by icariin and icariside II, J. Chin. Med. Mater. 33 (2010) 1896–1900.
[80] Z.Y. Jian, G.F. Xu, H.Z. Chen, et al., Study on the differences of major pharmaceutical ingredients in different parts and processed medicinal material of *Epimedium brevicornu* maxim in taihang mountain, Nutr. Hosp. 32 (2015) 913–917.
[81] Y. Chen, J.Y. Wang, X.B. Jia, et al., Role of intestinal hydrolase in the absorption of prenylated flavonoids present in Yinyanghuo, Molecules 16 (2011) 1336–1348.
[82] X. Wang, J.J. Li, L.F. Liu, et al., Pharmacological mechanism and therapeutic efficacy of icariside II in the treatment of acute ischemic stroke: A systematic review and network pharmacological analysis, BMC Complementary Med. Ther. 22 (2022), 18.
[83] R. Szabo, C.P. Racz, F.V. Dulf, Bioavailability improvement strategies for icariin and its derivates: A review, Int. J. Mol. Sci. 23 (2022) 7519.
[84] C.L. Feng, Y. Lu, Y.Y. Zhou, et al., Convenient preparation of 2''-o-rhamnosyl icariside II, a rare secondary flavonol glycoside, by recyclable and integrated biphase enzymatic hydrolysis, Phcog. Mag. 15 (2019) 147–155.
[85] J. Xie, H. Xu, J. Jiang, et al., Characterization of a novel thermostable glucose-tolerant GH1 β-glucosidase from the hyperthermophile ignisphaera aggregans and its application in the efficient production of baohuoside i from icariin and total epimedium flavonoids, Bioorg. Chem. 104 (2020), 104296.
[86] T. Cheng, J. Yang, T. Zhang, et al., Optimized biotransformation of icariin into icariside II by β-glucosidase from Trichoderma viride using central composite design method, BioMed Res. Int. 2016 (2016), 5936947.
[87] Y.P. Shen, M. Wang, J.W. Zhou, et al., Eco-efficient biphasic enzymatic hydrolysis for the green production of rare baohuoside I, Enzym. Microb. Technol. 131 (2019), 109431.
[88] Q. Li, L. Ge, D. Zheng, et al., Screening and characterization of a GH78 α-L-rhamnosidase from aspergillus terreus and its application in the bioconversion of icariin to icaritin with recombinant β-glucosidase, Enzym. Microb. Technol. 153 (2022), 109940.
[89] Q. Xia, D. Xu, Z. Huang, et al., Preparation of icariside ii from icariin by enzymatic hydrolysis method, Fitoterapia 81 (2010) 437–442.
[90] Q. Yang, L. Wang, L. Zhang, et al., Baohuoside I production through enzyme hydrolysis and parameter optimization by using response surface and subset selection, J. Mol. Catal. B Enzym. 90 (2013) 132–138.
[91] J.S. Park, H.Y. Park, H.S. Rho, et al., Statistically designed enzymatic hydrolysis for optimized production of icariside II as a novel melanogenesis inhibitor, J. Microbiol. Biotechnol. 18 (2008) 110–117.
[92] Y. Shen, H. Wang, Y. Lu, et al., Construction of a novel catalysis system for clean and efficient preparation of baohuoside I from icariin based on biphase enzymatic hydrolysis, J. Clean. Prod. 170 (2018) 727–734.
[93] L. Cui, Z. Zhang, E. Sun, et al., Effect of β-cyclodextrin complexation on solubility and enzymatic hydrolysis rate of icariin, J. Nat. Sci. Biol. Med. 4 (2013) 201–206.
[94] X. Jin, Z. Zhang, E. Sun, et al., Statistically designed enzymatic hydrolysis of an icariin/β-cyclodextrin inclusion complex optimized for production of icaritin, Acta Pharm. Sin. B 2 (2012) 83–89.
[95] X. Jin, Z.H. Zhang, E. Sun, et al., β-cyclodextrin assistant flavonoid glycosides enzymatic hydrolysis, Phcog. Mag. 9 (2013) S11–S18.
[96] L. Cheng, H. Zhang, H. Cui, et al., A novel α-L-rhamnosidase renders efficient and clean production of icaritin, J. Clean. Prod. 341 (2022), 130903.
[97] C.Y. Liu, R.Y. Li, J. Peng, et al., Enhanced hydrolysis and antitumor efficacy of epimedium flavonoids mediated by immobilized snailase on silica, Process Biochem. 86 (2019) 80–88.
[98] Y. Dong, S. Zhang, C. Lu, et al., Immobilization of thermostable β-glucosidase and α-l-rhamnosidase from dictyoglomus thermophilum DSM3960 and their cooperated biotransformation of total flavonoids extract from epimedium into icaritin, Catal. Lett. 151 (2021) 2950–2963.
[99] S. Zhang, J. Luo, Y. Dong, et al., Biotransformation of the total flavonoid extract of epimedium into icaritin by two thermostable glycosidases from dictyoglomus thermophilum DSM3960, Process Biochem. 105 (2021) 8–18.
[100] Y. Lyu, W. Zeng, G. Du, et al., Efficient bioconversion of epimedin C to icariin by a glycosidase from aspergillus nidulans, Bioresour. Technol. 289 (2019), 121612.

[101] R. Casella, D. Williams, S. Jambhekar, Solid-state β-cyclodextrin complexes containing indomethacin, ammonia and water. Ii. Solubility studies, Int. J. Pharm. 165 (1998) 15–22.
[102] S. Rawat, S.K. Jain, Solubility enhancement of celecoxib using β-cyclodextrin inclusion complexes, Eur. J. Pharm. Biopharm. 57 (2004) 263–267.
[103] H.R. Xi, H.P. Ma, K.M. Chen, et al., Preparation and characterization of icariin nanosuspension and lyophilized powder, China J. Chin. Mater. Med. 45 (2020) 4902–4908.
[104] X. Li, L. Hetjens, N. Wolter, et al., Charge-reversible and biodegradable chitosan-based microgels for lysozyme-triggered release of vancomycin, J. Adv. Res. 43 (2023) 87–96.
[105] X. Li, L. Kong, W. Hu, et al., Safe and efficient 2d molybdenum disulfide platform for cooperative imaging-guided photothermal-selective chemotherapy: A preclinical study, J. Adv. Res. 37 (2022) 255–266.
[106] X. Li, H. Sun, H. Li, et al., Multi-responsive biodegradable cationic nanogels for highly efficient treatment of tumors, Adv. Funct. Mater. 31 (2021), 2100227.
[107] R. Saka, N. Chella, Nanotechnology for delivery of natural therapeutic substances: A review, Environ. Chem. Lett. 19 (2021) 1097–1106.
[108] J. Nicolas, S. Mura, D. Brambilla, et al., Design, functionalization strategies and biomedical applications of targeted biodegradable/biocompatible polymer-based nanocarriers for drug delivery, Chem. Soc. Rev. 42 (2013) 1147–1235.
[109] G. Bozzuto, A. Molinari, Liposomes as nanomedical devices, Int. J. Nanomed. 10 (2015) 975–999.
[110] K. Tai, X. He, X. Yuan, et al., A comparison of physicochemical and functional properties of icaritin-loaded liposomes based on different surfactants, Colloids Surf., A 518 (2017) 218–231.
[111] J. Song, H. Huang, Z. Xia, et al., TPGS/phospholipids mixed micelles for delivery of icariside ii to multidrug-resistant breast cancer, Integr. Cancer Ther. 15 (2016) 390–399.
[112] C.F. Zhao, Z.H. Li, S.J. Li, et al., PLGA scaffold carrying icariin to inhibit the progression of osteoarthritis in rabbits, R. Soc. Open Sci. 6 (2019), 181877.
[113] H. Yan, Z. Zhang, X. Jia, et al., D-α-tocopheryl polyethylene glycol succinate/Solutol HS 15 mixed micelles for the delivery of baohuoside I against non-small-cell lung cancer: Optimization and *in vitro*, *in vivo* evaluation, Int. J. Nanomed. 11 (2016) 4563–4571.
[114] C. Tang, K. Meng, X. Chen, et al., Preparation, characterization, and *in vivo* evaluation of amorphous icaritin nanoparticles prepared by a reactive precipitation technique, Molecules 26 (2021), 2913.
[115] C. Tang, X. Chen, H. Yao, et al., Enhanced oral absorption of icaritin by using mixed polymeric micelles prepared with a creative acid-base shift method, Molecules 26 (2021), 3450.
[116] U. Kedar, P. Phutane, S. Shidhaye, et al., Advances in polymeric micelles for drug delivery and tumor targeting, Nanomed. Nanotechnol. Biol. Med. 6 (2010) 714–729.
[117] T. Toniazzo, I.F. Berbel, S. Cho, et al., Β-carotene-loaded liposome dispersions stabilized with xanthan and guar gums: Physico-chemical stability and feasibility of application in yogurt, LWT–Food Sci. Technol. 59 (2014) 1265–1273.
[118] S. Xia, S. Xu, Ferrous sulfate liposomes: Preparation, stability and application in fluid milk, Food Res. Int. 38 (2005) 289–296.
[119] L. Tu, Z. Liao, Z. Luo, et al., Ultrasound-controlled drug release and drug activation for cancer therapy, Explorations 1 (2021), 20210023.
[120] J. Hou, J. Wang, E. Sun, et al., Preparation and evaluation of icariside II-loaded binary mixed micelles using Solutol HS15 and Pluronic F127 as carriers, Drug Deliv. 23 (2016) 3248–3256.
[121] A. Dahan, A. Beig, D. Lindley, et al., The solubility–permeability interplay and oral drug formulation design: Two heads are better than one, Adv. Drug Deliv. Rev. 101 (2016) 99–107.
[122] X. Jin, Z.H. Zhang, E. Sun, et al., Preparation of a nanoscale baohuoside I-phospholipid complex and determination of its absorption: *in vivo* and *in vitro* evaluations, Int. J. Nanomed. 7 (2012) 4907–4916.
[123] J.W. Yoo, E. Chambers, S. Mitragotri, Factors that control the circulation time of nanoparticles in blood: Challenges, solutions and future prospects, Curr. Pharmaceut. Des. 16 (2010) 2298–2307.
[124] Y. Wei, L. Quan, C. Zhou, et al., Factors relating to the biodistribution & clearance of nanoparticles & their effects on *in vivo* application, Nanomedicine 13 (2018) 1495–1512.
[125] M.J. Mitchell, M.M. Billingsley, R.M. Haley, et al., Engineering precision nanoparticles for drug delivery, Nat. Rev. Drug Discov. 20 (2021) 101–124.
[126] S.Y. Fam, C.F. Chee, C.Y. Yong, et al., Stealth coating of nanoparticles in drug-delivery systems, Nanomaterials 10 (2020), 787.
[127] X. Li, L.X. Xing, K.L. Zheng, et al., Formation of gold nanostar-coated hollow mesoporous silica for tumor multimodality imaging and photothermal therapy, ACS Appl. Mater. Interfaces 9 (2017) 5817–5827.
[128] X. Li, Z.G. Xiong, X.Y. Xu, et al., ^{99m}Tc-l labeled multifunctional low-generation dendrimer-entrapped gold nanoparticles for targeted SPECT/CT dual-mode imaging of tumors, ACS Appl. Mater. Interfaces 8 (2016) 19883–19891.
[129] J.S. Brenner, S. MitragotriV, R. Muzykantov, Red blood cell hitchhiking: A novel approach for vascular delivery of nanocarriers, Annu. Rev. Biomed. Eng. 23 (2021) 225–248.
[130] D. Kalyane, N. Raval, R. Maheshwari, et al., Employment of enhanced permeability and retention effect (EPR): Nanoparticle-based precision tools for targeting of therapeutic and diagnostic agent in cancer, Mater. Sci. Eng., C 98 (2019) 1252–1276.
[131] H.M. Yan, J. Song, Z.H. Zhang, et al., Optimization and anticancer activity *in vitro* and *in vivo* of baohuoside I incorporated into mixed micelles based on lecithin and solutol hs 15, Drug Deliv. 23 (2016) 2911–2918.
[132] V.P. Chauhan, R.K. Jain, Strategies for advancing cancer nanomedicine, Nat. Mater. 12 (2013) 958–962.
[133] X. Li, M.S. Yang, X. Shi, et al., Effect of the intramolecular hydrogen bond on the spectral and optical properties in chitosan oligosaccharide, Phys. E 69 (2015) 237–242.
[134] X. Li, M.S. Yang, Z.P. Ye, et al., Dft research on the IR spectrum of glycine tryptophan oligopeptides chain, Acta Phys. Sin. 62 (2013), 156103.
[135] Z. Zhao, C. Chen, C. Xie, et al., Design, synthesis and evaluation of liposomes modified with dendritic aspartic acid for bone-specific targeting, Chem. Phys. Lipids 226 (2020), 104832.
[136] Y.L. Su, S.H. Hu, Functional nanoparticles for tumor penetration of therapeutics, Pharmaceutics 10 (2018) 193.
[137] L. Tang, N.P. Gabrielson, F.M. Uckun, et al., Size-dependent tumor penetration and *in vivo* efficacy of monodisperse drug–silica nanoconjugates, Mol. Pharm. 10 (2013) 883–892.
[138] J. Ding, J. Chen, L. Gao, et al., Engineered nanomedicines with enhanced tumor penetration, Nano Today 29 (2019), 100800.
[139] L. Tang, X. Yang, Q. Yin, et al., Investigating the optimal size of anticancer nanomedicine, Proc. Natl. Acad. Sci. USA 111 (2014) 15344–15349.
[140] Q. Sun, T. Ojha, F. Kiessling, et al., Enhancing tumor penetration of nanomedicines, Biomacromolecules 18 (2017) 1449–1459.
[141] M. Bartneck, H.A. Keul, S. Singh, et al., Rapid uptake of gold nanorods by primary human blood phagocytes and immunomodulatory effects of surface chemistry, ACS Nano 4 (2010) 3073–3086.
[142] L. Jia, X. Li, H. Liu, et al., Ultrasound-enhanced precision tumor theranostics using cell membrane-coated and ph-responsive nanoclusters assembled from ultrasmall iron oxide nanoparticles, Nano Today 36 (2021), 101022.
[143] E. Ruoslahti, Specialization of tumour vasculature, Nat. Rev. Cancer 2 (2002) 83–90.
[144] Y. Lu, A.A. Aimetti, R. Langer, et al., Bioresponsive materials, Nat. Rev. Mater. 2 (2016), 16075.
[145] X. Li, Z.J. Ouyang, H.L. Li, et al., Dendrimer-decorated nanogels: Efficient nanocarriers for biodistribution *in vivo* and chemotherapy of ovarian carcinoma, Bioact. Mater. 6 (2021) 3244–3253.
[146] X. Xue, X.J. Liang, Overcoming drug efflux-based multidrug resistance in cancer with nanotechnology, Chin. J. Cancer 31 (2012) 100–109.
[147] C. Yang, T. Wu, Y. Qi, et al., Recent advances in the application of vitamin E TPGS for drug delivery, Theranostics 8 (2018) 464–485.
[148] X. Li, S.Y. Lu, Z.G. Xiong, et al., Light-addressable nanoclusters of ultrasmall iron oxide nanoparticles for enhanced and dynamic magnetic resonance imaging of arthritis, Adv. Sci. 6 (2019), 1901800.
[149] X. Li, L.X. Xing, Y. Hu, et al., An rgd-modified hollow silica@au core/shell nanoplatform for tumor combination therapy, Acta Biomater. 62 (2017) 273–283.
[150] L. Gao, L. Feng, D.F. Sauer, et al., Engineered living hydrogels for robust biocatalysis in pure organic solvents, Cell Rep. Phys. Sci. 3 (2022), 101054.
[151] F. Xu, Q. Wu, L. Li, et al., Icariside II: Anticancer potential and molecular targets in solid cancers, Front. Pharmacol. 12 (2021), 663776.
[152] C. Zhang, X. Sui, Y. Jiang, et al., Antitumor effects of icaritin and the molecular mechanisms, Discov. Med. 29 (2020) 5–16.
[153] S. Sindhwani, W.C.W. Chan, Nanotechnology for modern medicine: Next step towards clinical translation, J. Intern. Med. 290 (2021) 486–498.
[154] I. de Lazaro, D.J. Mooney, Obstacles and opportunities in a forward vision for cancer nanomedicine, Nat. Mater. 20 (2021) 1469–1479.
[155] X. Li, H.L. Li, C.C. Zhang, et al., Intelligent nanogels with self-adaptive responsiveness for improved tumor drug delivery and augmented chemotherapy, Bioact. Mater. 6 (2021) 3473–3484.